POLITECNICO DI TORINO

MASTER's Degree in Mechatronic Engineering

MASTER's Degree Thesis

Model Based Virtual Sensing for Improved Vehicle Dynamic Testing

Supervisors

Prof. Stefano Alberto MALAN

Eng. Theo GELUK

Dr. Eng. Bart FORRIER

Candidate

Tommaso PIETRINI

July 2023

Summary

This thesis work was carried out for six months, as Test Division R&D intern of Siemens Digital Industries Software, located in Leuven, Belgium.

The accurate measurement of wheel forces is a crucial problem in the field of vehicle dynamics testing, as it directly impacts vehicle performance, handling and safety evaluations. Traditional methods, such as Wheel Force Transducers (WFTs), have limitations and require extensive modifications to the vehicle, making them impractical for routine testing. To address this challenge, model-based virtual sensing has emerged as a promising alternative solution.

Model-based virtual sensing involves two main steps: model development and estimation. Mathematical models of the vehicle and its components are created using techniques like multibody dynamics. These models incorporate the physical properties of tyres, suspension systems, and other factors to simulate the vehicle interaction with the road surface. Estimation algorithms, such as Kalman filters, are then employed to estimate the wheel forces by combining the developed models with available sensor measurements.

Past studies primarily relied on simplified models like the Single Track (Bycicle) model to estimate tyre forces. However, these models have limitations in accurately capturing tyre behavior due to assumptions of constant cornering stiffness and neglecting the influence of vertical forces. These limitations are reflected mainly in the large estimation errors during the build-up phase of the estimated lateral force. To overcome these limitations, researchers have explored more complex models, such as the 15 Degrees of Freedom (15DoFs) vehicle model, which enhances accuracy.

The framework for model-based virtual sensing encompasses several key components, including system modeling, estimation algorithms, testing/validation and observability analysis. System modeling involves mathematically representing the dynamics of the vehicle, considering subsystems like the powertrain, braking system, and suspension. Estimation algorithms, such as the Extended Kalman Filter (EKF), leverage the system model and available measurements to estimate unmeasured variables in real-time. Testing and validation activities are conducted to evaluate the performance of the framework by comparing estimated wheel forces against

reference data. Observability analysis plays a vital role in determining the states that can be accurately estimated based on available measurements, assisting in designing estimation algorithms and selecting appropriate sensor configurations.

The model of the system serves as estimator model: it receives as inputs the steering wheel angle and the longitudinal velocity and it provides the predicted states and outputs of the model to the estimator algorithm. In the 15DoFs vehicle model, the chassis model and tyre dynamics are key components. The chassis model represents the core of the model, integrating subsystems like the powertrain, suspension, braking and steering systems. It has been designed as an augmented states system because, besides the natural states, the cornering stiffnesses are added. Moreover other states (relative wheels angular displacements and steering rack displacement and velocity) presenting non-relevant dynamics have been fixed; it means excluding these states from the linearized matrices and then excluding from the estimator algorithm. It allows to have a reduced size system, speeding-up the algorithm, maintaining at the same time a robust framework. The tyre model plays a crucial role in the specific application. It is a linear adaptive tyre model, it means that the lateral load is linear with respect to the side-slip angle through the cornering stiffness and, moreover, the cornering stiffness is allowed to change, dynamically adapting in order to have the correct characteristic lateral force versus side-slip. The self-aligning torque is modeled as well. It is the torque generated (during streering) by the distribution of lateral force on the contact patch of the tyre, leading to align the wheel to the direction of motion. Overall, this model estimates lateral forces based on side-slip angles and dynamically adapts the cornering stiffness. Observability analysis employs various techniques, such as Popov-Belevitch-Hautus (PBH) analysis and Singular Value Decomposition (SVD), to assess the system observability:

- The PBH is a method to analyse local observability, so the observability of the system in a certain time instant. It is valid for linear systems, so in order to use it, the system considered in this work has to be linearized. The Jacobian matrices linearized around the true states of the system are considered.
- In order to extend to a global view, the SVD of a total observability matrix is introduced. The total observability matrix is nothing more than a collection of all the observability matrices for every time-step. Computing the SVD, if the system is unobservable, there will be at least one singular value close to zero. Doing that the matrix of right singular vectors can be split in an "observable part" and "unobservable part". The former can be used as a projection basis to project and modify the EKF algorithm allowing it to be stable even if the system is unobservable. The latter gives information on which states are unobservable.

These analyses highlight the loss of observability when the vehicle travels straight,

primarily due to unmeasurable cornering stiffnesses, but the EKF is stable in any case. Other two analyses are implemented more related to the sensors evaluation:

- The Fisher Information Matrix (FIM) is a statistical tool. Evaluating and comparing its metrics (Condition Number, Trace and Determinant) for different sensors sets, it gives an idea of the observability, sensitivity and uncertainty of each set. It can be proved that it corresponds to the inverse of state covariance matrix and so it is computed as Information Filter propagation in absence of process noise.

- The Sensitivity Indices (SI) give an image of how a certain measure is sensitive whit respect to the states of the system. Analyzing the measurement Jacobian matrix, it is possible to have a ranking of the relative importance, in state estimation, of the measures considered.

These analyses are useful if implemented for a simple system. For the considered system the FIM cannot be computed due to numerical errors and non-singular matrices; the SI are not trustworthy because they strongly depend on scaling or normalization matrices.

Sensors sets play a vital role in the framework, serving as inputs for the estimation algorithm. A gradual process of removing measures from a large set is employed to determine the optimal sensor set and the potential of the framework in having an accurate estimation even with a small number of measures. Economic and qualitative analysis, considering factors such as cost, instrumentation time, and availability, aids in ranking the sensors and selecting the best performing set.

The Estimator Model and the EKF algorithm are packed into a Functional Mock-up Unit in order to test the framework. To validate the framework, reference models are developed to generate (from simulation) sensor data for testing and validation. These models incorporate increased complexity, including the Dugoff tyre model and elastokinematics, to simulate realistic scenarios. The robustness of the framework is evaluated by considering expected modeling errors, such as variations in vehicle mass, center of gravity height and tyre stiffness.

The estimation results for the front and rear axle loads demonstrate the framework effectiveness. The errors over time are significantly reduced compared to the bicycle model, indicating improved accuracy. However, accuracy for the rear axle is slightly lower due to error propagation from the front axle. To address this, the EKF is tuned by adjusting the uncertainty of the rear cornering stiffness, resulting in enhanced estimation results. Increasing the uncertainty means let the cornering stiffness changing more and adapting in order to have more accurate results. The tuning phase results crucial because it allows to obtain promising estimation results even using a poor sensor set, with common measures. This proves the potential of the framework and the 15DoFs model.

Future research directions can focus on investigating variations in tyre model parameters, suspension characteristics and sensor calibration to improve the robustness and reliability of the virtual sensing algorithms. Additionally, the development of adaptive algorithms that can adjust model parameters based on online measurements and feedback can enhance estimation accuracy under varying operating conditions. Exploring advanced algorithms and sensor configurations for individual wheel force estimation can provide valuable insights into tyre-specific issues and contribute to targeted diagnostics and vehicle performance improvements. Experimental validation studies, utilizing controlled test setups and real-world vehicle testing, will further support and validate the proposed framework.

In conclusion, model-based virtual sensing presents a cost-effective, real-time and accurate solution for estimating wheel forces in vehicle dynamics testing. By eliminating the need for invasive modifications and providing real-time estimation capabilities, it surpasses traditional methods like WFTs. By integrating complex models, observability analysis and thoughtful sensor selection, it enables accurate and reliable estimation of unmeasured variables in complex systems. The framework potential lies in its ability to capture the intricate dynamics of the vehicle and its components, leading to a better understanding of vehicle behavior and aiding in vehicle development and testing processes.

Acknowledgements

I'd like to thank Prof. Malan for his significant support and insights that helped me write this work.

I am thankful to my supervisors Bart Forrier and Theo Geluk for creting the opportunity for this thesis. I am particularly grateful to Bart Forrier for his ongoing mentorship and for always expressing his confidence in my ability. His brilliant approach to work and research is an ispiration.

The thesis also marks the culmination of a journey, and it is only right to express gratitude to those who have shared it with you. To Alessandro, Davide, Emanuele, Gianmarco and Lorenzo my heartfelt thanks go out to you.

Of course, it is also essential to express my gratitude to my family. To my parents, who have always provided unwavering support and encouragement, and to my brother, who always knows how to bring a smile to my face.

Tommaso Pietrini

Table of Contents

List of Tables

List of Figures

Acronyms

WFT
Wheel Force Transducer

EKF
Extended Kalman Filter

FMI
Functional Mock-up Interface

FMU
Functional Mock-up Unit

SVD
Singular Value Decomposition

PBH
Popov–Belevitch–Hautus

FIM
Fisher Information Matrix

Chapter 1

Introduction

1.1 Problem Statement

In the field of vehicle dynamics testing, one crucial aspect is the measurement of wheel forces. Wheel forces are of significant importance in the dynamical testing of a vehicle as they provide essential data for evaluating performance, handling, and safety characteristics: they play a crucial role in assessing a vehicle performance, including acceleration, braking, and cornering capabilities. Monitoring wheel forces helps analyze a vehicle's handling and stability characteristics; they provide critical insights for evaluating vehicle safety (e.g. suspension problems can be detected) [1].

Wheel Force Transducers (WFTs [2]) have been widely used for this purpose, providing direct measurements of the forces exerted by each tire on the road surface. However, WFTs present several limitations and challenges that hinder their effectiveness in accurately capturing vehicle dynamics. The most relevant drawback regards the installation of WFTs on the vehicle: it requires significant modifications and alterations, often involving the removal of the tire and the integration of specialized sensors. This process is time-consuming and can cause additional costs, making it impractical for routine testing and evaluation scenarios.

Given the limitations of WFTs, there is a strong motivation to explore alternative approaches for acquiring accurate and reliable wheel force information. Model-based Virtual Sensing has emerged as a promising solution, aiming to estimate wheel forces through mathematical models and advanced estimation techniques, without the need for dedicated sensors. The motivation for adopting a virtual sensing approach is multifaceted. Firstly, it eliminates the need for invasive modifications to the vehicle, making it more convenient and cost-effective for both testing and production vehicles. Virtual sensing also enables real-time estimation of wheel forces, allowing for continuous monitoring and feedback during dynamic testing. Additionally, virtual sensing can leverage existing sensor measurements, such as

wheel speeds and vehicle accelerations, thereby utilizing the data already available in modern vehicle control systems.

1.2 Model-based Virtual Sensing

Model-based virtual sensing involves the development and utilization of mathematical models to estimate quantities that are difficult or expensive to measure directly. In the context of vehicle dynamics, this approach aims to estimate wheel forces and related parameters using a combination of vehicle models and measurement data [3]. By capturing the complex dynamics of the vehicle, these models provide insights into tire behavior and contribute to improved vehicle testing and development.

The virtual sensing process typically involves two main steps: model development and estimation [4]. In the model development phase, various techniques such as multibody dynamics, finite element analysis and system identification are employed to create accurate mathematical representations of the vehicle and its components. These models incorporate the physical properties of the tires, suspension system and other relevant factors to simulate the interaction between the vehicle and the road surface [5]. In the estimation phase, the developed models are combined with available sensor measurements, such as wheel speeds, accelerations and steering angles, to estimate the wheel forces. Advanced estimation algorithms, such as Kalman filters, particle filters or model predictive control, are employed to optimize the accuracy and robustness of the virtual sensing process [6]. The estimated wheel forces can then be used for various purposes, including vehicle development, performance evaluation and safety assessment.

1.3 Past Studies

In the past, researchers extensively utilized the commonly called bicycle model (Figure 1.1), a simplified representation of vehicle dynamics, to estimate tire forces and identify cornering stiffnesses. The model assumes that the vehicle can be represented as a single track with two wheels, neglecting the complexities of the suspension system and tire dynamics. While this model provides a simplified framework for analysis, it has limitations when it comes to accurately estimating tire forces. One of the primary challenges with the bicycle model approach is the assumption of constant cornering stiffnesses, which does not account for variations due to tire characteristics, road conditions or the nonlinear behavior of tires during dynamic maneuvers. This oversimplification can lead to inaccurate estimations and compromise the reliability of virtual sensing results. Furthermore, the single track model does not consider the influence of vertical forces on tire behavior. Vertical loads, which vary with vehicle dynamics and road surface irregularities,

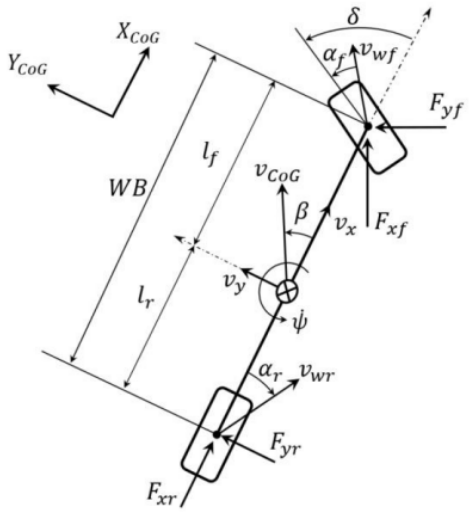

Figure 1.1: Single Track model

can significantly impact tire forces and cornering stiffnesses. Neglecting these effects in the estimation process limits the accuracy and applicability of virtual sensing techniques based on the bicycle model. More recent researches, tried to push the potentials of the single track model, in the field of tire load estimation and cornering stiffnesses identification, to the limit. An example is to combine the simple model with a so-called adaptive linear tire model (See section 4.2), enabling a better tracking of tire and vehicle dynamics across various operational conditions [7]. Regrettably, despite utilizing the finest single track model, three primary limitations are identified:

- The cornering stiffness estimation, thought the adaptive tire model, sometime diverges and it cannot catch the real behaviour.
- The accuracy of the axle loads estimation, in the transient, is too poor compared to the WFTs.
- Due to the simplicity of the model, it cannot catch particular dynamics in the transient. For example, monitoring the estimated axle loads, suspension parameters modifications are not captured.

These limitations prompt further exploration into utilizing more complex models. Initial attempts have indicated that a 15 Degrees of Freedom vehicle model could potentially enhance the accuracy and also pave the way for single wheel load estimation. Due to confidentiality, these limitations and potentialities are not documented in this work.

Chapter 2

Framework Presentation

2.1 Overview

As already said, a Model-based Virtual Sensing framework comprises several essential steps, each contributing to the overall process. The first step is system modeling, where the underlying dynamics of the system are captured and represented mathematically. This involves formulating equations that describe the relationships between the system's inputs, outputs and internal states.
The second step involves the estimation algorithm, which utilizes the system model to estimate the unmeasured or inaccessible variables of interest. In this case, an Extended Kalman Filter (EKF) was employed as the estimation algorithm. The EKF combines the system model and available measurements to provide estimates of the system states in real-time. By incorporating both system dynamics and measurement information, the EKF can compensate for uncertainties and noise in the sensor data, thereby improving the accuracy of the estimated states.
The third step is testing or validation, where the performance of the model-based virtual sensing framework is assessed. This involves evaluating the accuracy and reliability of the estimated wheel forces by comparing them against reference data. It helps to ensure that the framework operates effectively and provides reliable results under different operating conditions. Additionally, when dealing with complex systems, an important consideration is observability. In the context of state estimation, observability becomes crucial as it determines the feasibility and accuracy of estimating the complete set of states and consequently of the virtual sensors. By analyzing the observability of the system, one can identify which states can be accurately estimated and which ones may remain unobservable or poorly estimated. This analysis assists in designing effective estimation algorithms and selecting appropriate sensor configurations.

In the specific case discussed, the vehicle model was constructed using Simcenter

Amesim, a simulation software known for its capabilities in modeling complex physical systems. The EKF algorithm was developed using C++ in the Visual Studio environment, a popular integrated development environment (IDE) for software development. This combination of modeling software and programming tools allows for the creation of a reliable and efficient model-based virtual sensing framework for the vehicle system. In addition, the vehicle model and estimation algorithm are interfaced using the Functional Mock-up Interface (FMI) standard and packaged into a Functional Mock-up Unit (FMU). By utilizing the FMI standard, the FMU can be imported into simulation tools such as Testlab. Testlab provides a controlled environment for testing and validating the model-based virtual sensing framework. Within Testlab, the FMU can be connected to various input signals and simulated scenarios to assess the performance of the system model and estimation algorithm.

Overall, this framework integrates system modeling, estimation algorithms, testing and observability analysis to enable accurate and reliable estimation of unmeasured variables in complex systems.

2.2 Estimator Model

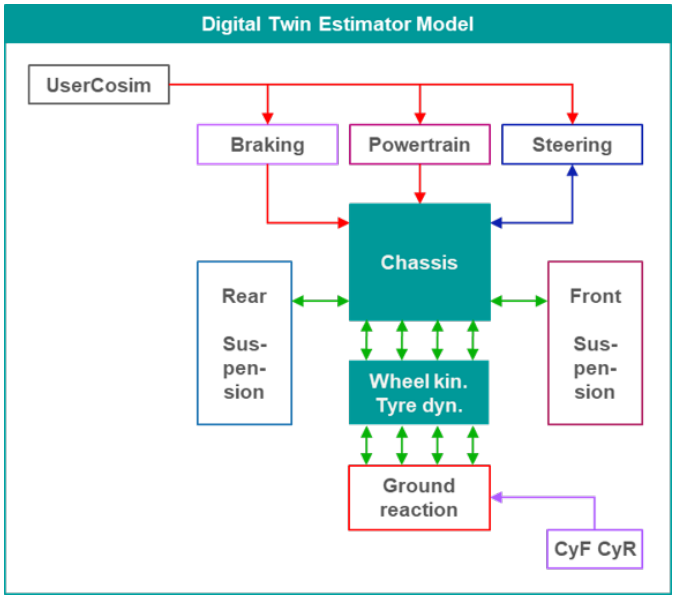

Figure 2.1: Vehicle Estimator Model Scheme

In model-based virtual sensing, an estimator model plays a crucial role in estimating or predicting unmeasured or difficult-to-measure variables or parameters based on available measurements. The estimator model utilizes mathematical

models and algorithms to infer the values of these variables by leveraging the relationships between measured variables and the target variables. As illustrated in Figure 2.1, the vehicle model consists of a Chassis model connected to various other components such as the suspensions model, the braking system, the powertrain, the steering system and the dynamics of the wheels and tires. This work focuses on modeling the chassis and the dynamics of the tires (see Chapter 4). The block labeled UserCosim enables co-simulation as stated by the FMU and in particular it represents the inputs provided to the model (in the specific case, the steering angle and the longitudinal velocity of the car).

2.3 EKF

This study utilizes an Extended Kalman Filter (EKF) as the central component of the state estimation process. This approach offers a favorable balance in addressing non-linear systems while facilitating a computationally efficient implementation [8]. Given a general non-linear system equations:

$$\text{Model:} \qquad \dot{\mathbf{x}} = \mathbf{f}(\mathbf{x}, \mathbf{u}, t) \tag{2.1}$$

$$\text{Measurements:} \qquad \mathbf{y} = \mathbf{h}(\mathbf{x}, t) \tag{2.2}$$

$$\text{Virtual Sensors:} \qquad \mathbf{y_{vs}} = \mathbf{g}(\mathbf{x}, t) \tag{2.3}$$

Let $\mathbf{x}$ denote the state vector, $\mathbf{u}$ the input vector and t represent the time. The vector $\dot{\mathbf{x}}$ represents the rate of change of the states over time, while the vectors $\mathbf{y}$ and $\mathbf{y_{vs}}$ correspond to the measurements and quantities of interest (virtual sensors), respectively. In order to evaluate the estimator, the linear and discrete Jacobian matrices are acquired by linearizing and discretizing the non-linear equations. The Jacobians are obtained through a linearization process centered around the a priori estimation point $(\hat{\mathbf{x}}_{k-1|k-1}, t_k)$ as follows:

$$\mathbf{F}_{c,k} = \left.\frac{\partial \mathbf{f}(\mathbf{x}, t)}{\partial \mathbf{x}}\right|_{\hat{\mathbf{x}}_{k-1|k-1}, t_k} \qquad \mathbf{H}_k = \left.\frac{\partial \mathbf{h}(\mathbf{x}, t)}{\partial \mathbf{x}}\right|_{\hat{\mathbf{x}}_{k|k-1}, t_k} \tag{2.4}$$

Then the exponential discretization scheme is used:

$$\mathbf{F}_k = e^{\mathbf{F}_{c,k}\Delta t} \tag{2.5}$$

Where $\mathbf{F}_k$ and $\mathbf{H}_k$ are the linearized and dicretized state transition Jacobian matrix and measurement Jacobian matrix respectively, $\mathbf{F}_{c,k}$ is the linearized continuous state transition Jacobian matrix and Δt is the step size. By utilizing the linearized Jacobians that were previously computed, we can establish the equations for the general estimator in Algorithm 1.

Algorithm 1 Extended Kalman Filter (EKF) Algorithm

Require: Initial state estimate $\hat{x}_0$, state covariance matrix P_0, process noise covariance matrix Q, measurement noise covariance matrix R

for $k = 1$ to N **do**
  Prediction Step:
    State Prediction: $\hat{\mathbf{x}}_{k|k-1} = \mathbf{f}(\hat{\mathbf{x}}_{k-1|k-1}, \mathbf{u}_k, t_k)$
    Covariance Prediction: $\mathbf{P}_{k|k-1} = \mathbf{F}_k \mathbf{P}_{k-1|k-1} \mathbf{F}_k^T + \mathbf{Q}$
  Update Step:
    Measurement Prediction: $\hat{\mathbf{y}}_k = \mathbf{h}(\hat{\mathbf{x}}_{k|k-1})$
    Kalman Gain Calculation: $\mathbf{K}_k = \mathbf{P}_{k|k-1} \mathbf{H}_k^T (\mathbf{H}_k \mathbf{P}_{k|k-1} \mathbf{H}_k^T + \mathbf{R})^{-1}$
    State Update: $\hat{\mathbf{x}}_{k|k} = \hat{\mathbf{x}}_{k|k-1} + \mathbf{K}_k (\mathbf{y}_k - \hat{\mathbf{y}}_k)$
    Covariance Update: $\mathbf{P}_{k|k} = (\mathbf{I} - \mathbf{K}_k \mathbf{H}_k) \mathbf{P}_{k|k-1}$
end for

The EKF-algorithm consists of two main steps:

1. Prediction Step:
   - State Prediction: The EKF uses the system nonlinear dynamic model to predict the state at the next time step $\hat{\mathbf{x}}_{k|k-1}$, given the previous state estimate $\hat{\mathbf{x}}_{k-1|k-1}$ and any known control inputs $\hat{\mathbf{u}}_k$. This prediction is represented by the state transition function $\mathbf{f}$.
   - Covariance Prediction: The EKF also predicts the covariance matrix $\mathbf{P}_{k|k-1}$, which represents the uncertainty in the state estimate. It accounts for the process noise introduced by the system dynamics $\mathbf{Q}$. The prediction is performed by linearizing the system's nonlinear equations using Jacobian matrices (2.5).
2. Update Step:
   - Measurement Prediction: In this step, the EKF uses the predicted state to generate expected measurements $\hat{\mathbf{y}}_k$ using the nonlinear measurement model. The measurement model describes how the state variables relate to the sensor measurements.
   - Kalman Gain Calculation: The Kalman Gain $\mathbf{K}_k$ determines the weight given to the predicted state estimate and the actual measurements. It is computed by combining the predicted covariance, the measurement model, and the measurement noise covariance $\mathbf{R}$.
   - State Update: The predicted state estimate is updated by combining the predicted state and the actual measurements $\mathbf{y}_k$ using the Kalman Gain. This step corrects the state estimate based on the new information from the sensors.

- Covariance Update: The covariance matrix is also updated based on the Kalman Gain. The update accounts for the uncertainty in the measurements and reduces the estimation error.

Considering the specific case of this framework, the State Prediction and the Measuremet Prediction steps (3 and 6 of Algorithm 1) are the tasks of the Estimator Model, that supplies the EKF-algorithm with these predicted quantities. Furthermore, in this work, the quantities of interest $\mathbf{y}_v s$ are governed by nonlinear equations (2.3). To approximate these quantities, a first-order Taylor expansion around a previously calculated state configuration $(\hat{\mathbf{x}}_{k+1|k+1}, t_k)$ is employed to derive their covariances. The approximation can be expressed as follow:

$$y_{vs} \approx g(x_{k|k}, t_k) + G_{vs,k}(x - x_{k|k}) + K_{vs,k}(t - t_k) \tag{2.6}$$

where $\mathbf{G}_{vs,k} = \frac{\partial \mathbf{g}(\mathbf{x},t)}{\partial \mathbf{x}}\Big|_{\hat{\mathbf{x}}_{k|k}}$ and $\mathbf{K}_{vs,k} = \frac{\partial \mathbf{g}(\mathbf{x},t)}{\partial \mathbf{t}}\Big|_{t_k}$ are the Jacobians of the quantity of interest. When evaluating Equation (2.6) around the current configuration point $(\hat{\mathbf{x}}_{k|k}, t_k)$ while assuming that the function g is approximately affine in this region, it can be stated that, up to a first-order approximation of the Taylor series, the quantities of interest will be a stochastic variable with the following mean and covariance:

$$\mathbf{y}_{vs,k} = \mathbf{g}(\hat{\mathbf{x}}_{k|k}, t_k) \tag{2.7}$$

$$\mathbf{P}_{vs,k} = \mathbf{G}_{vs,k}\mathbf{P}_{k|k}(\mathbf{G}_{vs,k})^T \tag{2.8}$$

2.4 FMU

The FMU serves as a self-contained software component that encapsulates the model and algorithm, allowing them to be easily exchanged and integrated into different simulation environments [9]. This approach offers flexibility and interoperability, as the FMU can be reused across different simulation platforms and environments that support the FMI standard. It enables efficient testing and validation of the model-based virtual sensing framework under various conditions, ensuring its robustness and reliability before implementation in real-world applications. Therefore, the use of the FMI standard and FMU packaging allows for seamless integration and thorough testing of the vehicle model and estimation algorithm within the Testlab environment, facilitating comprehensive evaluation and verification of the framework's performance. Figure 2.2 shows how the FMU is generated and tested in this work. In particular the framework is composed by at least three Amesim models, one for generating the sensors data, one used for the observability analysis and the Estimator Model. Three main Matlab files are used to generate the FMU:

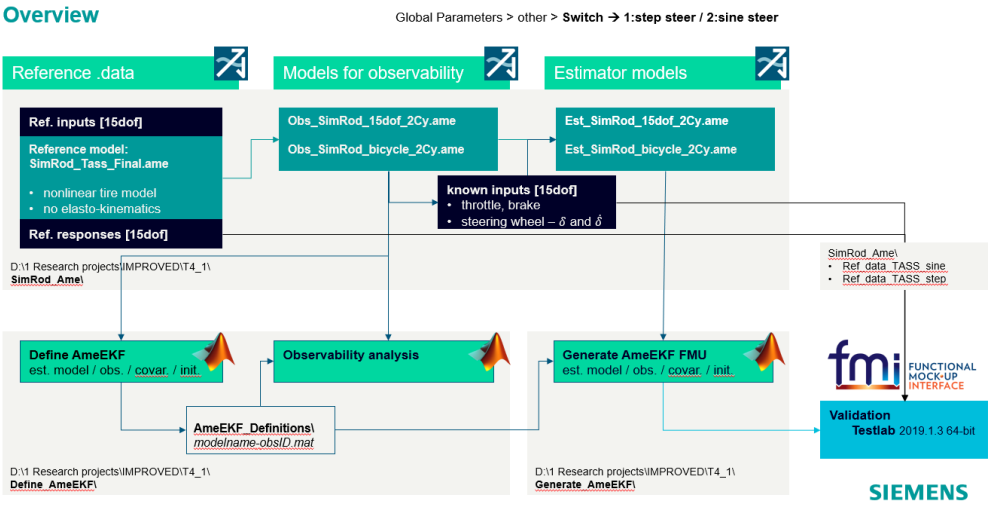

Figure 2.2: Overview of the framework for generating the FMU

- Define AmeEKF: It defines all the variables involved in the Model. It is based on the model for observability, that is a copy of the Estimator Model but without the UserCosim block, the inputs are directly provided to the model, it is a stand alone simulation model. the Matlab code obtains and stores all the states, inputs, outputs number, names and units and the unique variable identifire (a unique code for identifying a variable in a Amesim Model); it identifies the integrated states and the unknown inputs; the user can choose to analyze different cases, defining which are the sensors (observed variables) considered for every case; it defines the matrices $\mathbf{Q}$, $\mathbf{R}$ and the initialiations for the EKF; finally it generate a number of .mat definition files equal to the number of cases considered by the user.

- Observability Analysis: it does not interact directly with the FMU generation, it gives some information about the observability and the stability of the framework.

- Generate AmeEKF FMU: it generate effectively the FMU. it have as input the definition files from Define AmeEKF and it checks if all the variables are coherent with the Estimator Model; here the user defines which are the Virtual Sensors variables. Finally it pack together three main objects: an XML-file containing the definition of all variables of the FMU that are exposed to the environment in which the FMU will be utilized, along with other model information; a set of functions to set-up and properly run the model and the EKF-algorithm; the Estimator Model itself, some documentation files, the DLL (Dynamic-Link Library) that contains the C++ code in Visual studio

with the EKF-algorithm.

To conclude, in order to figure out what testing an FMU means, Figure 2.3 shows the scheme of the test process: the FMU receives some inputs, it runs internally its model and estimation algorithm and it provides some outputs. Looking now at

Figure 2.3: FMU testing: from inputs to outputs

Figure 2.4, it shows better how the FMU works internally: it receives as inputs the steering angle δ and the longitudinal velocity of the vehicle v_x, the Estimator Model acquires these data and gives as outputs the predicted states $\hat{\mathbf{x}}$ and observed variables $\hat{\mathbf{y}}$. These quantities are provided to the EKF algorithm with the sensors measurements y (FMU input), the matrices $\mathbf{Q}$ and $\mathbf{R}$ and the initializations $\mathbf{x}_0$, $\mathbf{P}_0$. The algorithm comes out with the updated states that are fed back to the estimator model to set these new states and to estimate the updated virtual sensors $\hat{\mathbf{y}}_{vs}$.

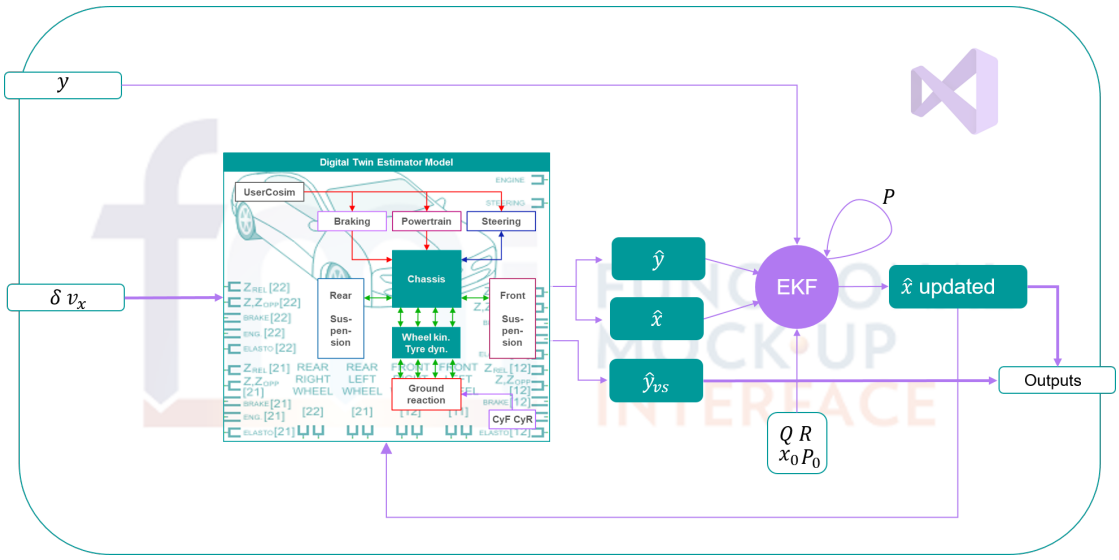

Figure 2.4: FMU internally work scheme

Chapter 3

Observability Analysis

Observability analysis plays a crucial role in the field of state estimation, providing insights into the ability to infer the complete internal state of a system based on the available measurements. State estimation refers to the process of estimating the unobservable or hidden variables within a system using measured data. These hidden variables are often critical for understanding and controlling complex systems. Observability, in the context of state estimation, refers to the extent to which the internal states of a system can be determined by its external outputs or measurements. A system is considered observable if, given sufficient measurements, it is possible to reconstruct the complete state accurately. Conversely, if certain states cannot be inferred from the measurements, the system is said to be unobservable. The concept of observability is closely related to controllability. While controllability deals with the ability to drive a system from one state to another using control inputs, observability focuses on the ability to determine the internal states based on the available measurements. Both concepts are fundamental to system analysis and control, with observability serving as a prerequisite for effective state estimation and control design. Observability analysis involves evaluating the observability properties of a system by examining its dynamics and measurement configurations. It aims to determine the set of states that can be accurately estimated based on the available measurements and identify any unobservable or poorly observable states. By analyzing observability, one can make informed decisions regarding sensor placement, measurement selection and control strategies to improve the accuracy and reliability of state estimation. Furthermore, observability analysis extends beyond linear systems and is applicable to nonlinear, time-varying, and stochastic systems. Nonlinear observability analysis deals with understanding the observability properties of systems with nonlinear dynamics, where traditional linear methods may not be directly applicable. Techniques such as nonlinear observers (EKF) have been developed to address the challenges of observability in nonlinear systems.

In conclusion, observability analysis is a vital aspect of state estimation. By evaluating the observability properties of a system, engineers can determine the extent to which the internal states can be accurately estimated based on the available measurements. This knowledge enables the design of effective state estimation algorithms, sensor configurations and control strategies, ultimately improving the performance and reliability of complex systems.

In this work, four different analyses have been implemented to examine observability:

- Popov–Belevitch–Hautus Analysis
- Singulat Value Decomposition of Total Observability Matrix
- Fisher Information Matrix
- Sensitivity Indices

The first two primarily address the quality and stability of the estimation, while the latter two focus on the influence that external measurements have on state estimation.

3.1 Popov-Belevitch-Hautus Analysis

The Popov-Belevitch-Hautus (PBH) analysis is a known method to get information about observability for linear systems. Given a LTI system in state space form (3.1)

$$\begin{aligned} \dot{\mathbf{x}} &= \mathbf{A}\mathbf{x} + \mathbf{B}\mathbf{u} \\ \mathbf{y} &= \mathbf{C}\mathbf{x} + \mathbf{D}\mathbf{u} \end{aligned} \tag{3.1}$$

a way to check the observability is checking the rank of a particular matrix:

$$rank \begin{bmatrix} \mathbf{A} - s\mathbb{I} \\ \mathbf{C} \end{bmatrix} \quad \forall s \; eig(\mathbf{A}) \tag{3.2}$$

If exists at least one eigenvalue for which the matrix is rank deficient, then the system is non-observable, moreover the number of unobservable modes are equal to the number of eigenvalues that make the matrix rank deficient [10].

In this work a complex and non-linear system is considered, all the aforementioned can be extended at this class of problem in different ways. In the specific case a linearization of the system around the true states is considered. The observability

analysis with this tool become a local observability analysis for a certain time instant checking the condition (3.3).

$$rank \begin{bmatrix} \mathbf{\Phi}_k - s\mathbb{I} \\ \mathbf{H}_k \end{bmatrix} \quad \forall s \; eig(\mathbf{\Phi}_k) \tag{3.3}$$

$\mathbf{\Phi}_k$ and $\mathbf{H}_k$ are the discretized Jacobians, linearized around the true state of the simulated system.

To resume, in this work the PBH test is used to check a local condition of observability for a certain time instant, using a linearized description of the system.

3.2 Singular Value Decomposition of Total Observability Matrix

Usually, the observability investigation starts with the standard observability criterion. Because of the non-linearity of the problem, the observability matrix $\mathbf{O}$ is the Kalman observability matrix [11] and it is based on the Jacobians $\mathbf{F_k}$ and $\mathbf{H_k}$ computed in Equations (2.5) and (2.4):

$$O = \begin{bmatrix} H_k \\ H_k F_k \\ H_k F_k^2 \\ \vdots \\ H_k F_k^{n-1} \end{bmatrix} \tag{3.4}$$

if the matrix is of full rank, meaning all its columns are linearly independent, then all the states of the system can be observed or estimated. Furthermore, this condition is sufficient for the estimator Riccati equation, a mathematical equation used in control systems estimation, to converge to a stable solution. While the condition mentioned above holds for local observability, which refers to observability within a specific region or neighborhood of the system operating point, global observability requires further analysis. Global observability considers observability across the entire state space of the system. The proposed approach in [12] involves combining observability matrices from different time steps into a single matrix. Each matrix represents the observability of the system at a specific time step. By combining these matrices, a comprehensive representation of the system observability across multiple time steps can be obtained. The matrices are evaluated at evenly spaced

time steps to ensure a representative coverage of the system dynamics:

$$O_{tot} = \begin{bmatrix} O_{k=1} \\ O_{k=1+p} \\ O_{k=1+2p} \\ \vdots \\ O_{k=N} \end{bmatrix} \tag{3.5}$$

where k is the evaluation time step, N is the total number of time steps and p is an integer, between 1 and N, that defines how many matrices are taken into account.

As for the local case, the rank of the O_{tot} has to be computed in order to say something about the global observability. It is known that a Singular Value Decomposition (SVD) can be employed to determine the rank:

$$O_{tot} = \mathbf{U}\mathbf{\Sigma}\mathbf{V}^T \tag{3.6}$$

where $\mathbf{\Sigma}$ is a square matrix having as the main diagonal the singular values while matrices $\mathbf{U}$ and $\mathbf{V}$ contain the corresponding modes. If O_{tot} is rank deficient, at least one of the singular value is close to zero, the structure of $\mathbf{\Sigma}$ becomes:

$$\mathbf{\Sigma} = \begin{bmatrix} \sigma_1 & \dots & 0 & 0 & \dots & 0 \\ \vdots & \ddots & \vdots & \vdots & \ddots & \vdots \\ 0 & \dots & \sigma_m & 0 & \dots & 0 \\ 0 & \dots & 0 & \approx 0 & \dots & 0 \\ \vdots & \ddots & \vdots & \vdots & \ddots & \vdots \\ 0 & \dots & 0 & 0 & \dots & \approx 0 \end{bmatrix} = \begin{bmatrix} \Sigma_o & \dots & 0 \\ \vdots & \ddots & \vdots \\ 0 & \dots & \Sigma_u \end{bmatrix} \approx \begin{bmatrix} \Sigma_o & \dots & 0 \\ \vdots & \ddots & \vdots \\ 0 & \dots & 0 \end{bmatrix} \tag{3.7}$$

where m is the number of non zero singular values σ_i, so the rank of the total observability matrix O_{tot}. Having the relation stated in (3.7), the matrix of right singular vectors $\mathbf{V}$ can be split:

$$\mathbf{V}^T = \begin{bmatrix} \mathbf{V}_o \\ \mathbf{V}_u \end{bmatrix} \tag{3.8}$$

where $\mathbf{V}_u$ is the matrix containing the modes that span the kernel of O_{tot}, corresponding to the zero singular values. Analyzing the components of these modes, in particular looking at which component is zero or not, one can determine which states are unobservable [13] and consequently cause the instability of the estimation.

3.2.1 Projection to an Observable Subspace

With estimation instability, it means practically that some elements of the covariance matrix $\mathbf{P}$ become unbounded and they increase, introducing huge errors in the estimation.

The proposed approach in [12], suggests to consider $\mathbf{V}_o$ in relation (3.8), the matrix containing the modes corresponding to an observable subspace of the system (with the defined sensors set), as a projection basis to obtain a totally observable system and a stable estimator. The new linearized Jacobians become:

$$\widetilde{\mathbf{F}}_k = \mathbf{V}_o \mathbf{F}_k \mathbf{V}_o^T \tag{3.9}$$

$$\widetilde{\mathbf{H}}_k = \mathbf{H}_k \mathbf{V}_o^T \tag{3.10}$$

As a consequence, using the SVD and (3.7), the new total observability matrix is:

$$O_{tot}\mathbf{V}_o^T = \mathbf{U}\mathbf{\Sigma}\mathbf{V}^T\mathbf{V}_o^T = \mathbf{U}\begin{bmatrix}\Sigma_o & 0\\ 0 & 0\end{bmatrix}\begin{bmatrix}\mathbf{V}_o\\ \mathbf{V}_u\end{bmatrix}\mathbf{V}_o^T \tag{3.11}$$

then, these relations can be proved:

$$\mathbf{V}_u\mathbf{V}_o^T = 0 \tag{3.12}$$

$$\mathbf{V}_o\mathbf{V}_o^T = \mathbb{I} \tag{3.13}$$

Now, using (3.12) and (3.13) in (3.11), the following relation is obtained

$$O_{tot}\mathbf{V}_o^T = \mathbf{U}\begin{bmatrix}\mathbf{\Sigma}_o\\ 0\end{bmatrix} \tag{3.14}$$

(3.14) proves that the new observability matrix is of full rank.

The proposed approach leads to a modified version of Kalman Filter Algorithm, with projected equations, showed in Algorithm 2

Algorithm 2 Projected Extended Kalman Filter (EKF) Algorithm

1: **for** $k = 1$ to N **do**
2: **Prediction Step:**
3: $\hat{\mathbf{x}}_{k|k-1} = \mathbf{f}(\hat{\mathbf{x}}_{k-1|k-1}, \mathbf{u}_k, t_k)$
4: $\mathbf{P}_{k|k-1} = (\mathbf{V}_o\mathbf{F}_k\mathbf{V}_o^T)\mathbf{P}_{k-1|k-1}(\mathbf{V}_o\mathbf{F}_k\mathbf{V}_o^T)^T + (\mathbf{V}_o\mathbf{Q}_k\mathbf{V}_o^T)$
5: **Update Step:**
6: $\hat{\mathbf{y}}_k = \mathbf{h}(\hat{\mathbf{x}}_{k|k-1})$
7: $\mathbf{K}_k = \mathbf{P}_{k|k-1}(\mathbf{H}_k^T\mathbf{V}_o)((\mathbf{H}_k\mathbf{V}_o)\mathbf{P}_{k|k-1}(\mathbf{H}_k\mathbf{V}_o)^T + \mathbf{R})^{-1}$
8: $\hat{\mathbf{x}}_{k|k} = \hat{\mathbf{x}}_{k|k-1} + \mathbf{V}_o^T\mathbf{K}_k(\mathbf{y}_k - \hat{\mathbf{y}}_k)$
9: $\mathbf{P}_{k|k} = (\mathbf{I} - \mathbf{K}_k(\mathbf{H}_k\mathbf{V}_o^T))\mathbf{P}_{k|k-1}$
10: **Quantities of Interest:**
11: $\mathbf{y}_{vs,k} = \mathbf{g}(\hat{\mathbf{x}}_{k|k}, t_k)$
12: $\mathbf{P}_{vs,k} = (\mathbf{G}_{vs,k}\mathbf{V}_o^T)\mathbf{P}_{k|k}(\mathbf{G}_{vs,k}\mathbf{V}_o^T)^T$
13: **end for**

Due to the projection, the covariance matrix $\mathbf{P}_{k|k}$, computed at step 9, is not anymore full size, but it is of size m, according to (3.7). As a result, the unobservable states are excluded from the covariance equations, allowing them to remain stable.

3.3 Fisher Information Matrix

The Fisher Information Matrix (FIM) is a fundamental concept in statistics and estimation theory. It measures the amount of information that an observed data set carries about unknown parameters in a statistical model. The FIM plays a crucial role in understanding the observability of a system. In the context of observability, the FIM is used to assess whether the parameters of a dynamic system can be uniquely estimated or "observed" from the available measurements. It is defined, in statistics, as the variance of the score function related to the estimation problem [14].

The approach proposed in [14] consists in computing the FIM for different sets of sensors and investigate three characteristics of this matrix:

1. The condition number (CN) is defined as the ratio of the largest singular value to the smallest singular value (3.15). It is closely related to the rank of a matrix and reflects the difficulty of performing matrix inversion. When the number of rows (m) is smaller than the number of columns (n), the rank of the FIM is at best equal to m, and minimizing the condition number helps achieve this. By minimizing the condition number, redundancy among sensors can be avoided, ensuring that no sensor provides redundant information compared to another.

$$CN(FIM) = \frac{\sigma_{max}}{\sigma_{min}} \tag{3.15}$$

2. The trace (Tr) of the FIM is defined as the sum of the singular values (3.16). In the case where m is smaller than n, the sum is limited to the first m singular values. The trace represents the overall sensitivity of the sensors with respect to the parameters and therefore should be maximized.

$$Tr(FIM) = \sum_{i=1}^{m} \sigma_i \tag{3.16}$$

3. The determinant (Det) of the FIM is defined as the product of the singular values (3.17). Similarly, the product is restricted to the first m singular values. Since, as mentioned in point 1, at most m singular values are nonzero, this quantity should be maximized. The inverse of the determinant serves as a measure of the overall uncertainty in the estimated parameters.

$$Det(FIM) = \prod_{i=1}^{m} \sigma_i \tag{3.17}$$

Furthermore, the following relation, called the Cramér-Rao inequality, states:

$$\mathbf{P} \geq \mathbf{P}^* \triangleq \mathbf{I}^{-1} \tag{3.18}$$

where $\mathbf{P}$ is the covariance matrix defined in Algorithm 1, $\mathbf{I}$ is the FIM and $\mathbf{P}^*$ is the "best can be done" in terms of performance of an EKF. More important is that the inverse FIM can be computed following the same equations of covariance matrix EKF propagation [15]. Thus, the following relation is defined:

$$\mathbf{I}_{k|k} = (\mathbf{\Phi}_{k|k-1}^{-1})^T \mathbf{I}_{k|k-1} \mathbf{\Phi}_{k|k-1}^{-1} + \mathbf{H}_k^T \mathbf{R}^{-1} \mathbf{H}_k \tag{3.19}$$

where $\mathbf{\Phi}$ and $\mathbf{H}$ are the Jacobian matrices linearized around the true states of the system (not around the estimated states as in the classical EKF). The relation (3.19) equals the propagation of the inverse of the covariance matrix in the Information Filter (a variant of EKF) [8] in absence of process noise (when $\mathbf{Q}$ is set to zero).

In conclusion, in this work, the FIM is computed as EKF propagation of the inverse of covariance matrix considering different sensors sets, so different measurements, and then, comparing the characteristic metrics (CN, Tr, Det) of the different FIMs, the sets of measures can be evaluated.

3.4 Sensitivity Indices

Other tools to evaluate the importance of measures in the estimation are the so called Sensitivity Indices SI. They give an image of how a certain measure is sensitive whit respect to the states of the system [14]. The indications given by the FIM are with respect to different sensors set, now this tool open the possibility to rank a given measure (sensor) based on its contribution on the states estimation. To analyze the relation between states and measure, considering that the system is non-linear, the measurement Jacobian matrix $\mathbf{H}$ is considered, actually a scaled version $\mathbf{G} = (\sqrt{\mathbf{R}})^{-1}\mathbf{H}$ is used. $\mathbf{G}$ takes into account the relative accuracy of each sensor. Computing the SVD:

$$\mathbf{G} = \mathbf{U}\mathbf{\Sigma}\mathbf{V}^T \tag{3.20}$$

Giving a practical interpretation of (3.20), $\mathbf{G}$ maps the space of states to the space of measures, while looking at the SVD, it is a sort of change of reference frame in the spaces of input and output. In the new representation, the columns of $\mathbf{V}$ represent the frame of states, the columns of $\mathbf{U}$ represent the frame of measures and $\mathbf{\Sigma}$ is the mapping. Having this new interpretation the SI can be computed as:

$$SI_i = \mathbf{U}_i \sqrt{\Sigma\Sigma^T} \mathbf{U}_i^T \qquad i = 1...n_s \tag{3.21}$$

where $\mathbf{U}_i$ are the columns of $\mathbf{U}$ form (3.20) and the number of SI is equal to the number of measures (sensors) n_s. Obviously this analysis is performed considering the system with the largest sensor set, considering all possible measures available.

3.5 Simple 3DoF System Example

In this section an example of the observability analysis will be performed on a simple system composed by three masses linked by two nonlinear springs, as depicted in Figure 3.1. In the system considered $m_1 = m_2 = m_3$, $k_1 = k_2$, the inputs are

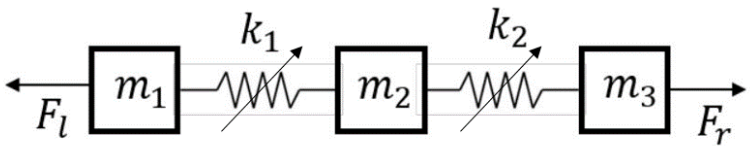

Figure 3.1: 3DoF system composed by masses and non-linear springs

symmetrical sinusoidal excitation $F_l = F_r$, the states of the system are clearly all the positions and velocities of the masses $[\dot{x}_1\ x_1\ \dot{x}_2\ x_2\ \dot{x}_3\ x_3]$. Three sensors sets are considered: one that measures only the position of the inner mass, the second measures all the positions, the last measures all the accelerations (Table 3.1).

Table 3.1: Sensors Sets building for 3DoF system

	Sensors Set
1	x_2
2	$x_1\ x_2\ x_3$
3	$\ddot{x}_1\ \ddot{x}_2\ \ddot{x}_3$

Firstly the PBH test can be performed, instead of computing the rank, the maximum condition number for the initial and final time of simulation of the PBH matrices is considered (Figure 3.2). The results are clear for the sensor set configurations 1 and 2 (x_2 and x_{all}), that is the system is observable considering measuring all the positions, while is non-observable measuring only the position of the inner mass. The results are not clear for the sensor set configuration 3, when all the accelerations are measured. This ambiguity can be solved computing the SVD of the total observability matrix. Looking at the singular values (Figure 3.3), it is now clear that the cases 2 and 3 lead to an observable system, while considering the set 1, two singular values are close to zero, so two unobservable modes are present.

It is important spending a couple of words on the system when the sensors set 1 is used. If the system have as input a symmetric excitation, the inner mass is not moving, while the outer masses move in an opposite way. Thus, measuring only the position of the inner mass do not give information about the other two masses, then it is for definition an unobservable system. This unobservability has been confirmed by the two analysis aforementioned, but it is important to show the effect on the

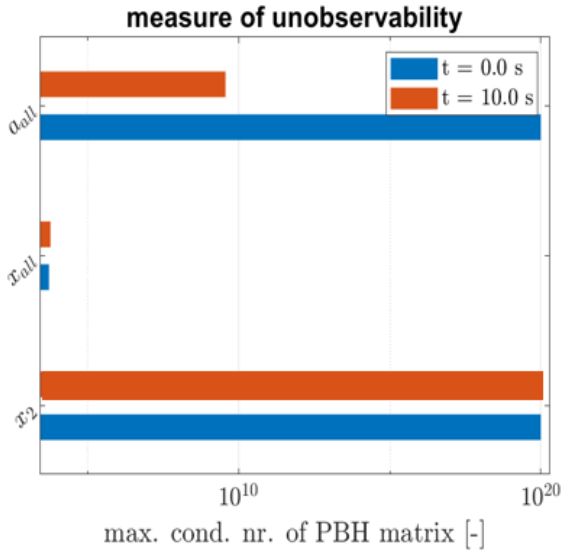

Figure 3.2: PBH analysis. Condition numbers plotted for the three cases (x_2, x_{all}, a_{all}) at time $t = 0s$ and $t = 10s$

estimation stability and the potentiality of the projection approach proposed in section 3.2.1. In Figure 3.4 the variance of the states (diagonal terms of $\mathbf{P}$ matrix) is plotted, without the projection and with the projection. If the projection is not applied, the variances relative to the states of the outer masses are unbounded and they increase, leading the EKF algorithm to instability and affecting the estimation. When the projection to the observable subspace is applied, the effect on variances is clearly visible in Figure 3.5, in which the curves relative to the projection are zoomed in, they are stable and lower in magnitude. The variances associated to x_2 and $\dot{x}_2$ do not change with the projection, the states associated to the inner mass, in this configuration are observable. In order to go into more details on this aspect, the components of the right singular vectors (related to the unobservable modes) are investigated. Table 3.2 shows that the components of last two singular vectors, different from zero, are the once referring to the states of outer masses, so the unobservable ones.

Table 3.2: Singular vector components related to unobservable modes considering Set 1

Singular Vectors - Set 1						
v_5	-0.002	-0.707	0	0	0.002	0.707
v_6	-0.707	0.002	0	0	0.707	-0.002
State	x_1	$\dot{x}_1$	x_2	$\dot{x}_2$	x_3	$\dot{x}_3$

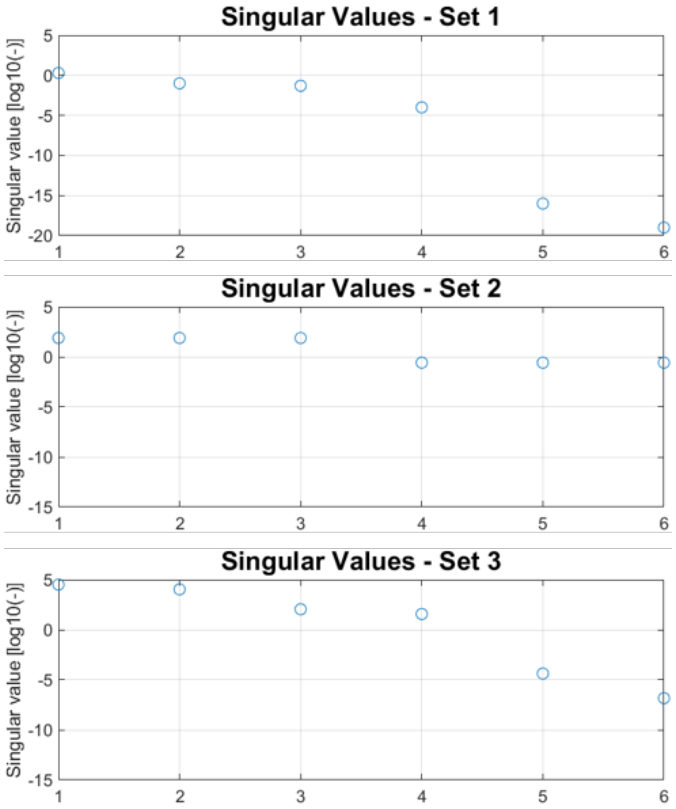

Figure 3.3: SVD(O_{tot}). Singular values for the three sensors sets considered

Until now, the observability of the system has been investigated. Involving the FIM and SI, the sensor side analysis related to quality of estimation can be accomplished as well, having a complete idea of what is the best configuration in terms of observability, sensors involved and quality of estimation. In Figure 3.6 the parameters of the FIM (CN, Tr, Det) are compared with respect to the three sensors sets used. If for the condition number there are no differences, the third sensor set (all the accelerations) have better performance concerning the trace and determinant because these metrics have to be maximized, as explained in section 3.3. In order to have an idea of which sensor is more sensitive to the state estimation with respect to others, the sensitivity indices can be computed. In Table 3.3 are listed the indices, ranked from the highest to the lowest, conferring a relative importance to the acceleration measures.

In order to resume, given the system depicted in Figure 3.1, built the three sensors sets in Table 3.1, the observability analysis is conducted using all the tools introduced in chapter 3. It came out that the best configuration of the system in view of state estimation is measuring all the accelerations: the system is observable (the ambiguity from the PBH analysis is solved by considering the total

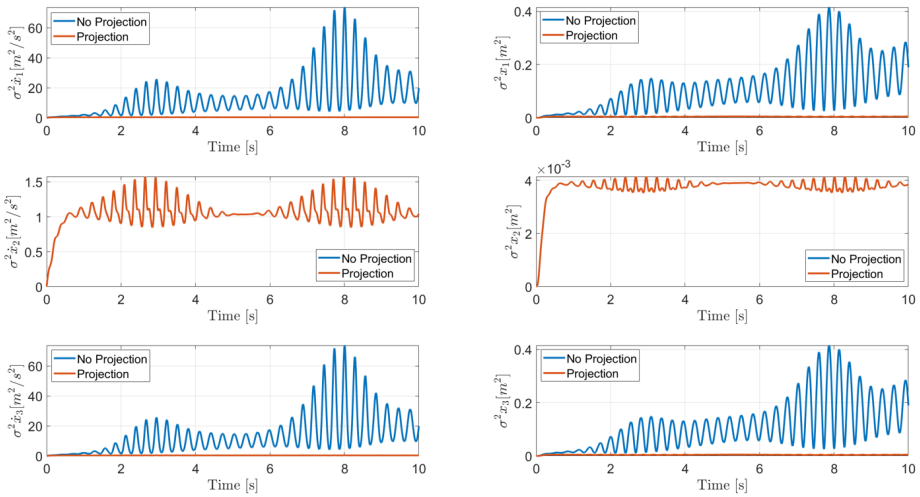

Figure 3.4: Variances associated to the states for the 3DoF system with and without the projection approach

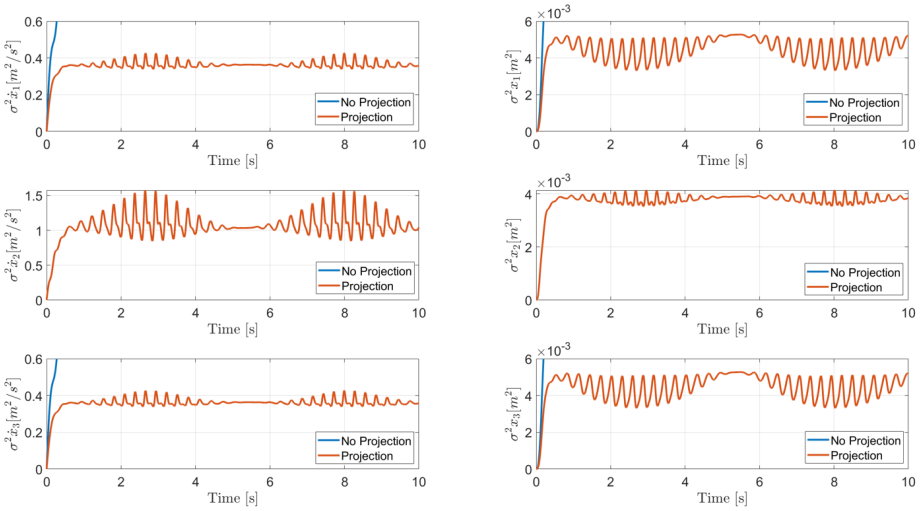

Figure 3.5: Zoom of variances associated to the states for the 3DoF system whit projection approach

observability matrix) and measuring acceleration is the best set of sensors in terms of sensitivity to the states and uncertainty.

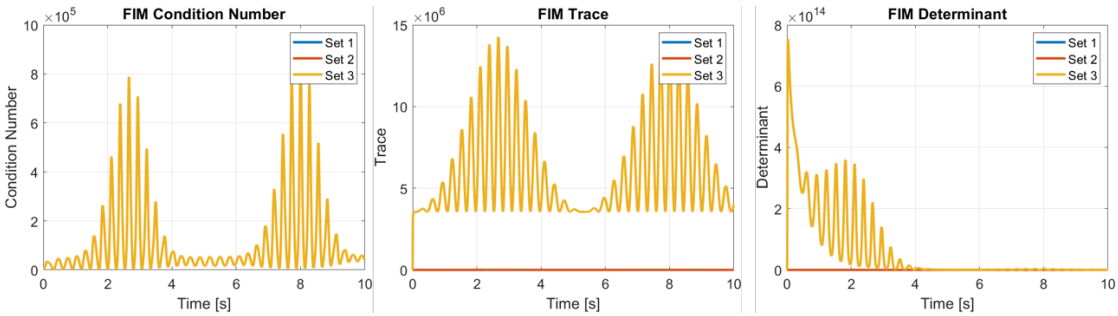

Figure 3.6: FIM condition number, trace and determinant for the three sensors sets considered

Table 3.3: Sensitivity Indices for 3DoF system

Sensor	SI
$\ddot{x}_2$	853.57
$\ddot{x}_1$	426.78
$\ddot{x}_3$	426.78
x_1	1.07
x_3	1.07
x_2	1.06

Chapter 4

15 DoFs Model

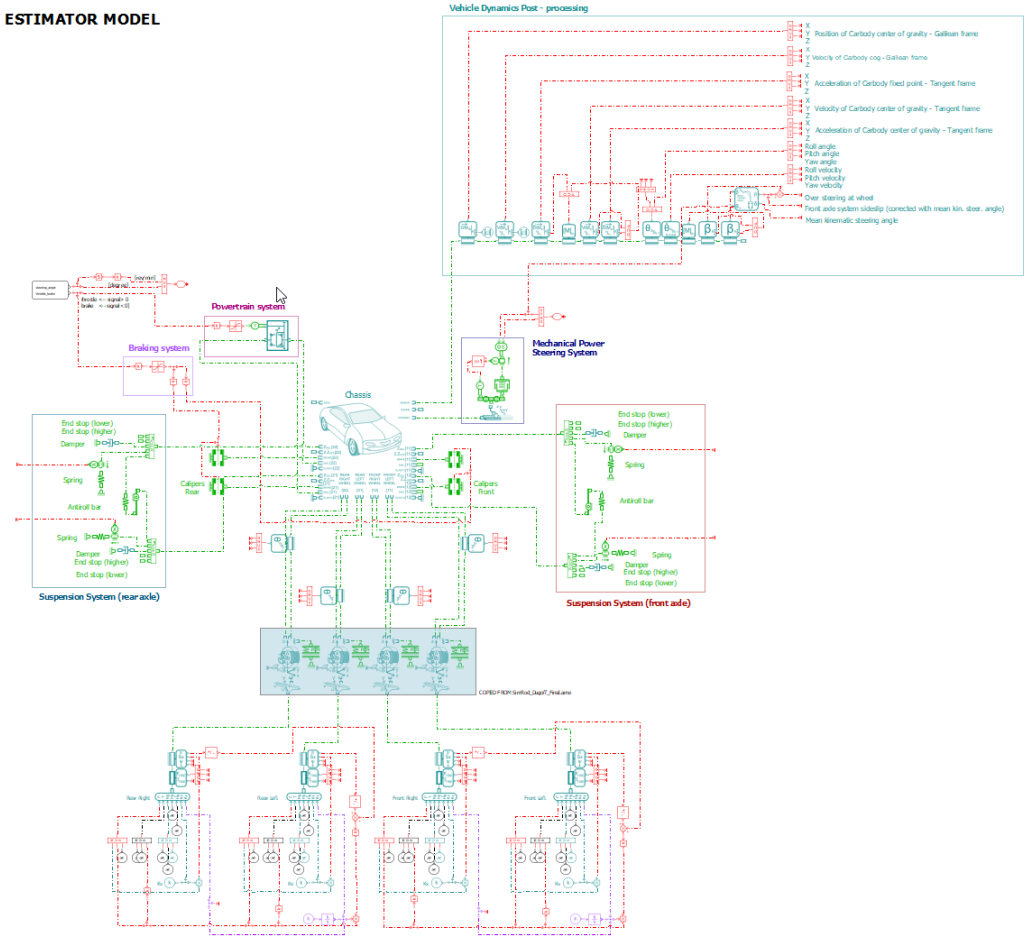

Figure 4.1: 15 DOFs model developed in Simcenter Amesim

The 15 degrees of freedom model is the so called Estimator Model or digital twin. It is a numerical model developed in Simcenter Amesim that takes into account the kinematics and the dynamics of a simplified vehicle model in order to predict the states, the outputs and the virtual sensors quantities. The model (Figure 4.1) is composed by a multibody 15 DoFs chassis to which all the subsystems are linked: the powertrain system, the braking system, the mechanical power steering system, the suspension systems rear and front axle, the kinematic and dynamic tyre models, sensors if needed. This work focuses its attention on the chassis, defining the states of the system, and on the tire model, fundamental in order to estimate the forces in the tyre-road contact.

4.1 Chassis

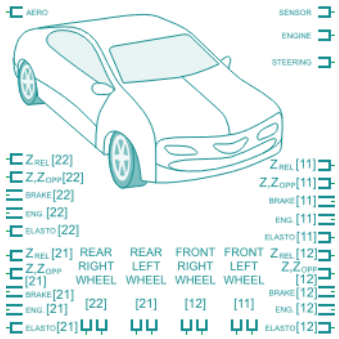

Figure 4.2: Multibody 15 DoFs chassis block on Amesim

The chassis is the core of the model, it takes as inputs all the kinematic quantities by the subsystems (Figure 4.2). In this work the chassis is a 15 DoFs model. The degrees of freedom are depicted in Figure 4.3 and they are: x_G, y_G, z_G position of center of gravity; ϕ, θ, ψ roll, pitch and yaw angles; $\theta_{rel11}, \theta_{rel12}, \theta_{rel21}, \theta_{rel22}$ the relative angles of the front-left, front-right, rear-left, rear-right wheel respectively; $z_{rel11}, z_{rel12}, z_{rel21}, z_{rel22}$ the relative displacements of the spindles; y_{crav} the steering rack displacement. Normally in the state space representation, the states are the degrees of freedom plus their derivatives, resulting in this case thirty states. Actually the real size of the system considered is twenty-four for two reasons:

- Two augmented states are added, the cornering stiffnesses front and rear (C_{yF}, C_{yR}); they are fundamental in order to precisely estimate the axle lateral forces. Identifying these two quantities in the state estimation, the dynamics of the tyres are better captured.
- $x_G, y_G, \theta_{rel11}, \theta_{rel12}, \theta_{rel21}, \theta_{rel22}, y_{crav}, \dot{y}_{crav}$ are selected as fixed states. Fixing some states in Amesim means excluding these states from the linearization; it

allows to exclude (possible unobservable) non-relevant dynamics. As a result the system size is reduced, the EKF algorithm is sped up and it permits to exclude some measurements, such as the steering rack displacement and velocity that are difficult and expensive to measure.

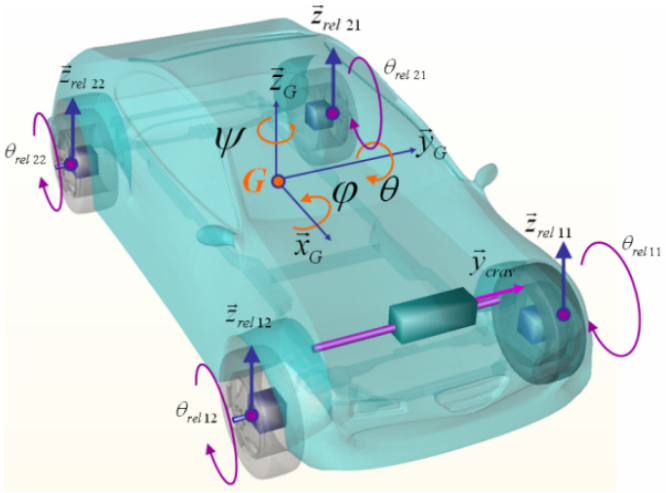

Figure 4.3: 15 DoFs Vehicle Model

The system inputs (steering angle δ and longitudinal velocity v_x), and states are summarized in the Table 4.1

Table 4.1: Inputs and states of the 15DoFs model

Inputs	States
δ	$\dot{x}_G\ \dot{y}_G\ \dot{z}_G\ z_G\ \dot{\phi}\ \dot{\theta}\ \dot{\psi}\ \phi\ \theta\ \psi\ \dot{z}_{rel11}\ z_{rel11}\ \dot{\theta}_{rel11}\ \dot{z}_{rel12}, z_{rel12}$
v_x	$\dot{\theta}_{rel12}\ \dot{z}_{rel21}, z_{rel21}\ \dot{\theta}_{rel21}\ \dot{z}_{rel22}\ z_{rel22}\ \dot{\theta}_{rel22}\ C_{yF}\ C_{yR}$

4.2 Linear Adaptive Tyre Model

The linear adaptive tyre method bases its model on the relation between the lateral force $\mathbf{F}_y$, acting on the tyre, and the wheel side-slip angle β. The general expressions for this kind of model are:

$$\mathbf{F}_y = C_y \beta \tag{4.1}$$

$$\frac{dC_y}{dt} = 0 \tag{4.2}$$

where C_y is the cornering stiffness, it represents the tyre resistance to lateral force during cornering maneuvers. The side-slip angle β represents the sideways deformation of the tyre from its intended direction of motion as depicted in Figure 4.4 The relation (4.1) states for the linear part of the model, because the lateral

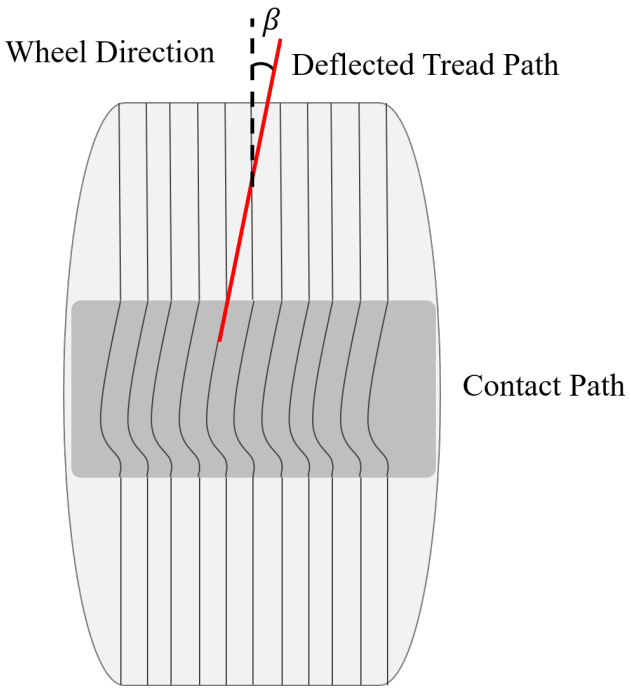

Figure 4.4: Deformation of a tyre and Side-slip angle

load is linearly dependent to the side-slip angle; the relation (4.2) consider the adaptive part, it defines a random walk model that in practice allows the cornering stiffness to change (Figure 4.5) . Using the EKF framework, the cornering stiffness is adapted dynamically based on the measured data. It allows the model to better track the dynamics [7].

In this work, the model in Figure 4.6 is considered, but the focus is not on the individual forces, but on the lateral axle loads front and rear, so the following relation states for the tyre models:

$$\bar{\beta}_1 = \frac{\beta_{11} + \beta_{12}}{2} \qquad \bar{\beta}_2 = \frac{\beta_{21} + \beta_{22}}{2} \tag{4.3}$$

$$\mathbf{F}_{y11} = \mathbf{F}_{y12} = C_{y1}\bar{\beta}_1 \qquad \mathbf{F}_{y21} = \mathbf{F}_{y22} = C_{y2}\bar{\beta}_2 \tag{4.4}$$

$$\mathbf{M}_{z11} = \mathbf{M}_{z12} = C_{y1}\bar{\beta}_1\epsilon \qquad \mathbf{M}_{z21} = \mathbf{M}_{z22} = C_{y2}\bar{\beta}_2\epsilon \tag{4.5}$$

In (4.3) $\bar{\beta}_1$ and $\bar{\beta}_2$ are the mean values of the individual side-slip angles front an rear respectively. Since the interest is on the total lateral load, in the relation (4.4),

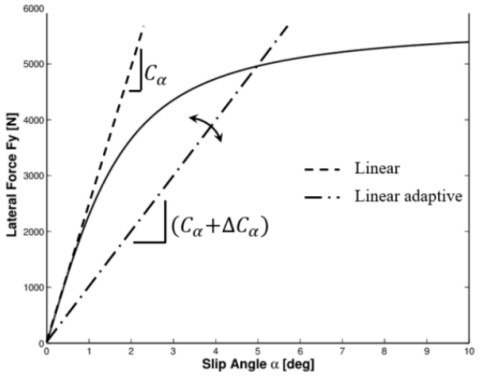

Figure 4.5: Characteristic Lateral Force vs Side-slip [7]. The cornering stiffness C_α is the slope of the linear part considering a linear tyre model, if the model is linear adaptive, it can vary.

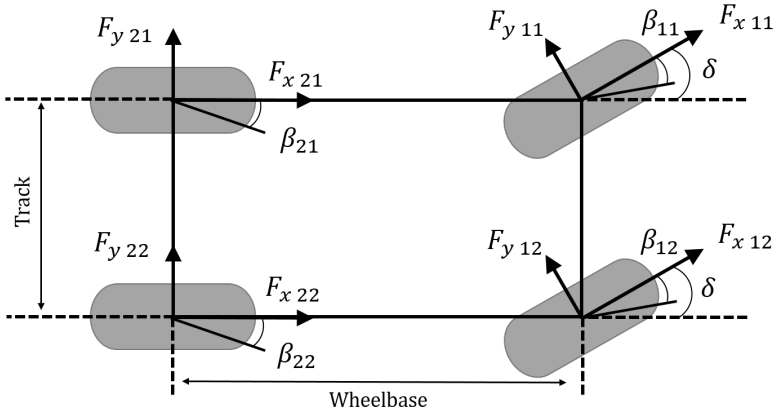

Figure 4.6: Scheme of the vehicle model with forces and angles

the individual wheel lateral loads are considered equal in right and left side and proportional to the mean side-slip angles. In this model the self-aligning moments $\mathbf{M}_{zii}$ are modeled as well. They are the torques, developed by the tyres while cornering, that tend to align the wheel plane with the vehicle direction of motion. $\mathbf{M}_z$ is computed basically multiplying the lateral force by the pneumatic trail ϵ (relation (4.5)) that is caused by the force build-up: the distribution of lateral force in the contact patch have as a resultant a force shifted by ϵ from the center of the wheel (Figure 4.7). The relations (4.3), (4.4), (4.5) are implemented in the Amesim model as showed in Figure 4.8.

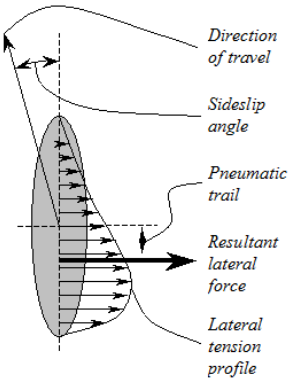

Figure 4.7: The distribution of lateral force in the contact path shifts the resultant lateral force by the pneumatic trail.

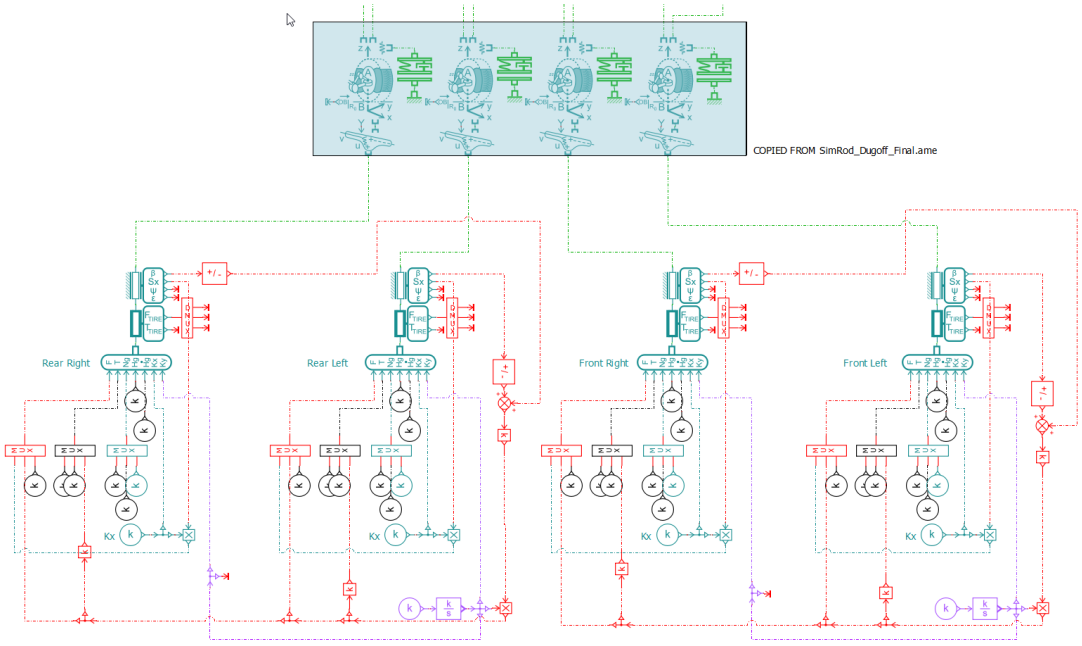

Figure 4.8: Amesim implementation of tyre model.

Chapter 5

Reference Models

The reference models are numerical models, developed in Simcenter Amesim, whose purpose is to generate sensors data (and reference signals to compare with estimated as well). As explained in Chapters 1 and 2, the inputs of the frameworks are the sensors measures, normally they come from a test campaign in which an instrumented vehicle is drove through different maneuvers. This work is an early analysis about the potentiality of the 15DoFs model in tire load estimation with respect to the widely used "Bicycle Model"; for that reason, data from a test campaign were not available. Different models had been built, with increasing complexity, in order to validate the framework. To obtain higher complexity, three solutions are adopted:

- A more complex tyre model is used, like the Dugoff model.
- The Elastokinematics is added to the wheel model.
- Some expected modelling errors are included.

5.1 Dugoff Tyre Model

The Figure 5.1 shows an overview of the reference model. Comparing with the estimator model in Figure 4.1, it is visible that, overall, the model is the same, but two elements are different: there is not the FMI block, because this is a stand-alone model that has to simulate the system response; more important is that the model of tyres is changed (at the bottom of the Figure 5.1). In this case the model implemented is the Dugoff tyre model, that generates the tire contact force at the tyre-road interface. This force modeling is based on a macroscopic and phenomenological theory developed by Howard Dugoff [16]. The Dugoff tire model builds upon the original Coulomb's friction theory and introduces a more

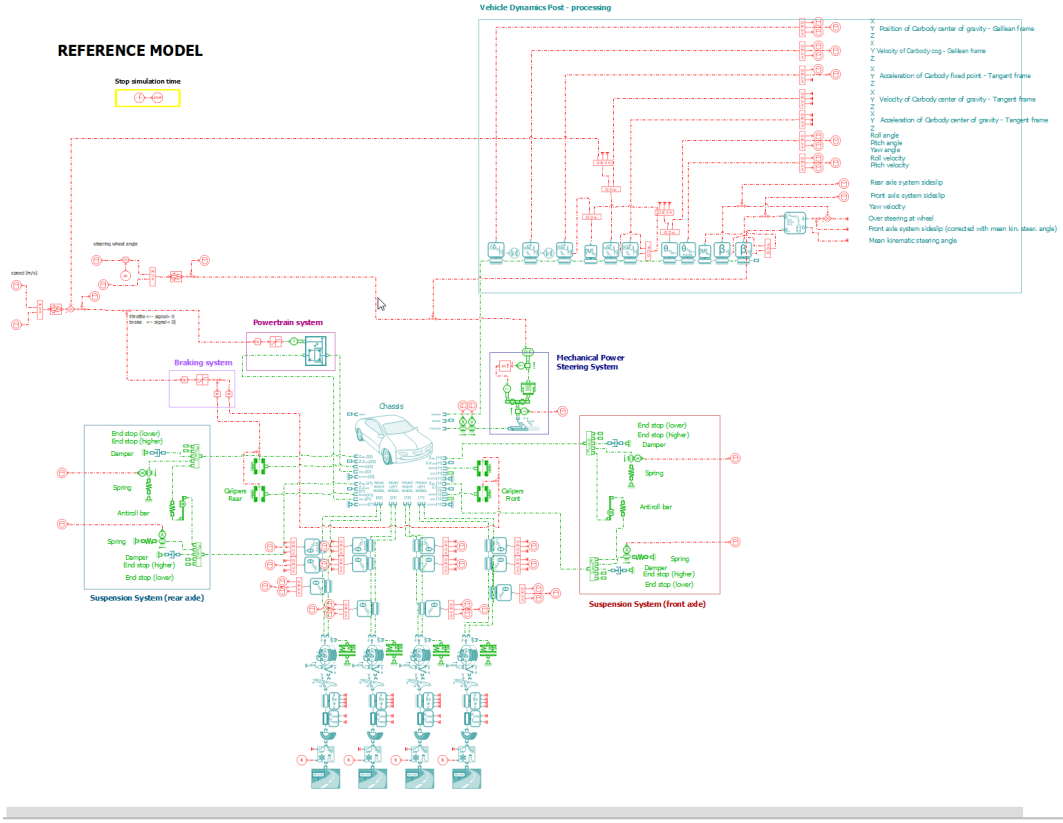

Figure 5.1: Reference model with Dugoff tyre

realistic concept called elliptical adherence. This concept is visualized through curves representing iso-side slip and iso-longitudinal slip at a specific vertical load 5.2. In these curves, the module of the tangential lateral force component decreases while the longitudinal force component increases. The Dugoff tire model expands upon Coulomb's friction theory by providing a characterization of tire traction and lateral shear forces as functions of the tire/road friction coefficient (μ) and the vertical load applied to the contact patch ($\mathbf{F}_z$). In Figure 5.3 the characteristics of lateral (longitudinal) force versus side (longitudinal) slip angle are shown. It is visible that for a certain range of slip angles, the relation is linear and the slope is the cornering stiffness, then increasing the slip angle there is a saturation and the relation becomes non-linear. The curves of different colors shows that increasing the vertical load obviously, the longitudinal and lateral forces increase in magnitude as well.

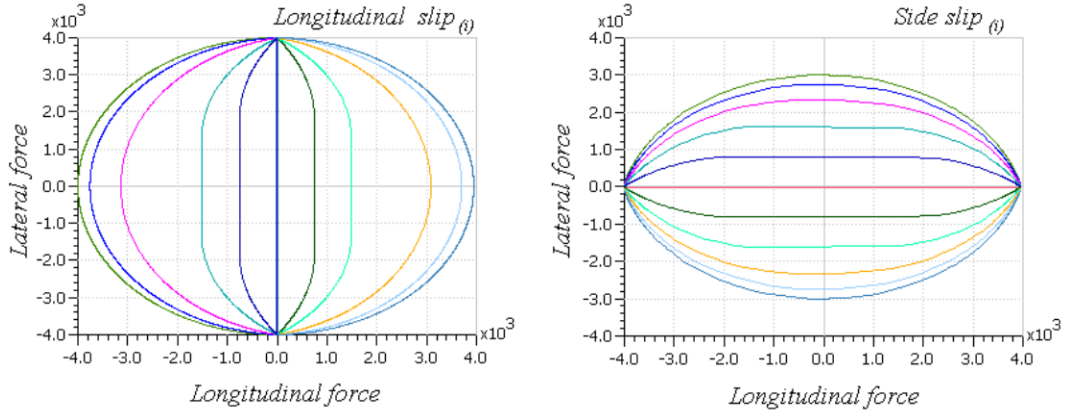

Figure 5.2: Lateral load vs longitudinal force for a given vertical load, curves iso-longitudinal slip angle (left graph) and iso-side-slip angle (right graph)

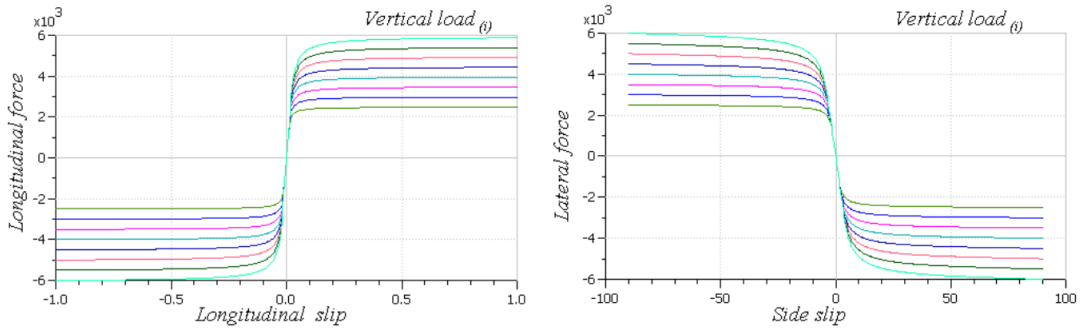

Figure 5.3: Characteristics of Dugoff tyre model: longitudinal force vs longitudinal slip angle (left) and lateral force vs side-slip angle (right)

5.2 Elatokinematics

Figure 5.4 shows the reference model, developed in Amesim, in which Dugoff tyre model and elastokinematics are modeled in order to take into account more complexity. The elastokinematic model is a computational framework used to determine the elastic displacement of a wheel in response to the constraint forces exerted by the axle system. This displacement includes both the elastic displacement of the wheel center and the elastic angular displacement of the rim plane. When a load is applied, the axle system exhibits flexibility, leading to elastic deformations in the wheel. These deformations are quantified using an analytical linear formulation, which takes into account the properties of the axle system, such as its stiffness and compliance. The elatokinematic model is seen as a flexibility component, providing

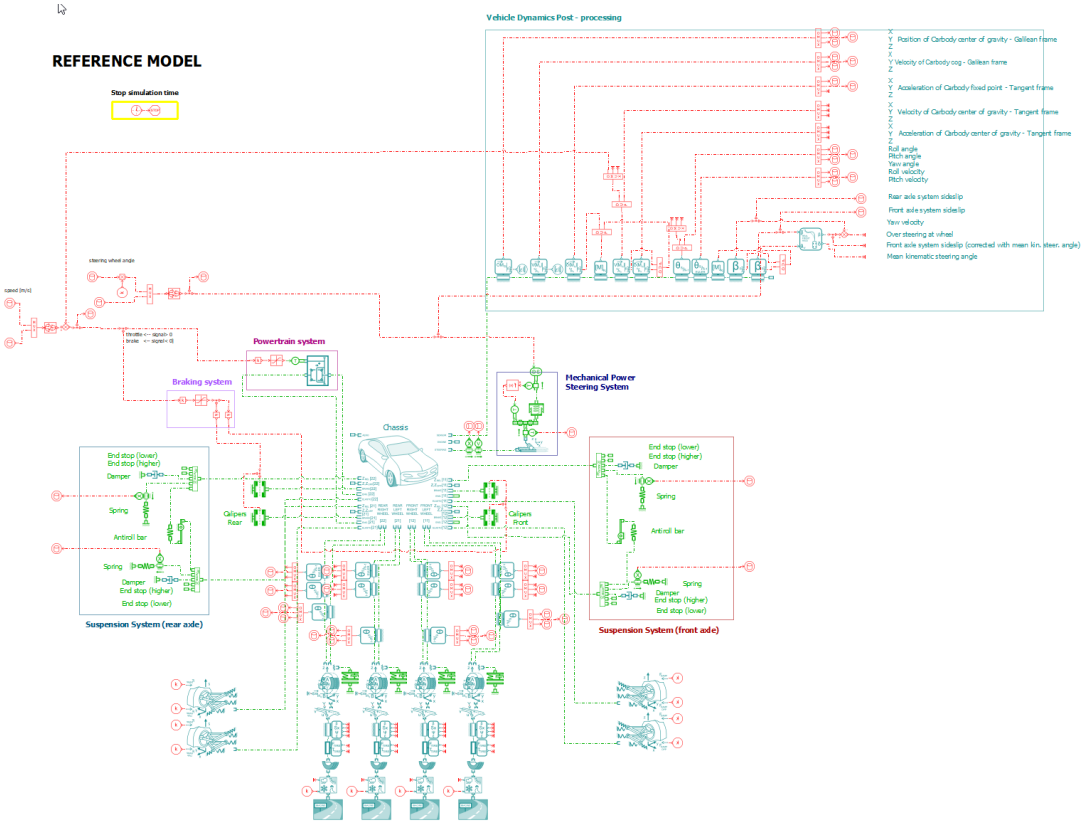

Figure 5.4: Reference model with Dugoff tyre and Elastokinematics

displacement from an effort:

$$d\mathbf{x} = \begin{bmatrix} dx_{elas} \\ dy_{elas} \\ d\epsilon_{elas} \\ d\eta_{elas} \\ d\delta_{elas} \end{bmatrix} = [\mathbf{S}] \begin{bmatrix} F_x \\ F_y \\ M_\epsilon \\ M_\eta \\ M_\delta \\ F_{damp} \end{bmatrix} = \mathbf{F} \tag{5.1}$$

with $dx_{elas}, dy_{elas}, d\epsilon_{elas}, d\eta_{elas}, d\delta_{elas}$ being respectively the longitudinal displacement, the lateral displacement, camber angle, self rotating angle and steering angle due to elastic effects. The elastic induced displacements depend on five constraint efforts: two forces on x and y axis (F_x, F_y), three moments around x, y and z axis $(M_\epsilon, M_\eta, M_\delta)$ and force in damper elements (F_{damp}). $[\mathbf{S}]$ is the flexibility matrix. Furthermore, the elastokinematic effects formulation introduces an implicit formulation of the elastic deformation under load:

$$d\mathbf{x} = [\mathbf{S}]\mathbf{F}(x) \tag{5.2}$$

This implicit formulation (5.2) leads to algebraic loops on each component of induced displacement vector $d\mathbf{x}$; the model used provides the dynamic of elastic deformation employing a second order lag formulation as follow;

$$\ddot{x} = 2\pi\omega_n(2\pi\omega_n(x_{in} - x) - 2\zeta\dot{x}) \tag{5.3}$$

with: x is the elastic displacement part of elatokinematic effect, with respect to derivatives $\dot{x}$ and $\ddot{x}$; x_{in} is the elastic displacement part of elatokinematic effect computed with flexibility matrix, considered input of the second order lag; ω_n and ζ are the natural frequency and damping ratio of the second order lag respectively. All the information about elastokinematics are taken from a Simcenter Amesim guide for the specific component.

5.3 Expected Modelling Errors

In order to validate the framework, some expected modelling errors are considered in the reference models. The aim is to test if the framework is robust with respect to this common expected errors.

When constructing a vehicle model, it is important to recognize that there may be certain modeling errors associated with various parameters. Three significant parameters that can introduce modeling errors in a vehicle model are:

- Mass of the Vehicle ($M_{vehicle}$): The accurate determination of the vehicle mass is crucial for dynamic analysis and simulation. Modeling errors in the mass estimation can arise due to uncertainties in the weight distribution, the inclusion of additional equipment or modifications or incomplete knowledge of the vehicle components. These errors can affect the vehicle acceleration, braking, and handling characteristics.

- Height of the Center of Gravity (z_{CoG}): The vertical position of the center of mass has a substantial impact on a vehicle stability and handling. Inaccuracies in estimating the height of the center of mass can arise from assumptions about the distribution of mass within the vehicle or errors in measuring the position of heavy components. Incorrect estimation of the center of mass height can lead to inaccurate predictions of vehicle roll, pitch and stability during maneuvers.

- Vertical Tire Stiffness (K_{tyre}): The stiffness of the tires is a critical parameter in vehicle modeling, affecting the vehicle ride comfort, handling and tire-road interactions. Modeling errors in tire stiffness can occur due to variations in manufacturing tolerances, changes in tire pressure or inaccurate characterization of the tire material properties. These errors can affect the accuracy of

simulations related to tire forces, vehicle response to steering inputs and the prediction of tire slip behavior.

From the experience, the errors are quantified in Table 5.1. They are applied individually, one by one, on the reference model with only the Dugoff tyres (Figure 5.1).

Table 5.1: Expected modelling errors

Parameter	Percentage Error (%)
$M_{vehicle}$	± 5
z_{CoG}	± 5
K_{tyre}	± 20

Chapter 6

Sensors Sets Building

Building the sensors sets is a fundamental phase of the work in a model-based virtual sensing approach. Their signals are the inputs of the framework and they are compared with the predicted outputs (coming from the estimator model) in order to properly update the states in the EKF algorithm. These measures normally are acquired with a test campaign, in this work synthetic data, generated by simulation of reference models, are used.

Having a performing sensors set lead the estimation to accurate values of states and virtual sensors, so it is important to have all the measures that help the EKF algorithm to have good performances; at the same time it is worth considering sensors that are cheap in terms of time of instrumentation and money. For this reason a simple economical and qualitative analysis has been developed: a large number of sensors are listed and ranked basing on the economical cost of the sensors, the cost and time of instrumentation and the availability in a hypothetical common costumer. In Table 6.1 all the sensors considered are listed and they are ranked in three categories; from standard to advance the cost of the sensors and the instrumentation cost and time increase, while the availability in a costumer decreases. The approach used to build the sensors sets consists in going from a large set to a small set, gradually removing measures. Five sensors sets are built, starting from considering all the measures and then removing measures in order to obtain reduced sets. The aim is to test the framework with all the sets in order to see the potentiality: how far can we push cutting out measures while still getting reliable results? In Table 6.2 all the information about the measures considered and the composition of the sets are summarized. In particular the table shows: the economic/qualitative category associated to measures; the measures are grouped with respect to the physical sensor employed (IMU, GPS,...); there is a column containing the standard deviation values associated to each measure, the values are computed plotting all the simulated reference signals and taking the 0.05% of the maximum range. These uncertainties correspond to the values (squared) present

Table 6.1: Sensors list ranked by three categories: standard (S), medium (M), advance (A)

Category	Sensor Measures	Symbols
S	Absolute Velocity of CoG	$\dot{x}_G \dot{y}_G \dot{z}_G$
	Absolute Vertical Position of CoG	z_G
	Carbody Roll, Pitch, Yaw rate	$\dot{\phi}\dot{\theta}\dot{\psi}$
	Carbody Roll, Pitch, Yaw angle	$\phi\theta\psi$
	Carbody Longitudinal Acceleration	a_x
	Carbody Lateral Acceleration	a_y
	Carbody Front Axle Slip Angle	β_1
	Carbody Rear Axle Slip Angle	β_2
	Steering Torque	T_δ
M	Toe, Camber, Self-rotating Angle front-left wheel	$\delta_{11}\epsilon_{11}\eta_{11}$
	Toe, Camber, Self-rotating Angle front-right wheel	$\delta_{12}\epsilon_{12}\eta_{12}$
	Toe, Camber, Self-rotating Angle rear-left wheel	$\delta_{21}\epsilon_{21}\eta_{21}$
	Toe, Camber, Self-rotating Angle rear-right wheel	$\delta_{22}\epsilon_{22}\eta_{22}$
	Vertical Relative Displacement of front-left Suspension	z_{rel11}
	Relative Rotary Velocity of front-left wheel	$\dot{\theta}_{rel11}$
	Vertical Relative Displacement of front-right Suspension	z_{rel12}
	Relative Rotary Velocity of front-right wheel	$\dot{\theta}_{rel12}$
	Vertical Relative Displacement of rear-left Suspension	z_{rel21}
	Relative Rotary Velocity of rear-left wheel	$\dot{\theta}_{rel21}$
	Vertical Relative Displacement of rear-right Suspension	z_{rel22}
	Relative Rotary Velocity of rear-right wheel	$\dot{\theta}_{rel22}$
A	Side-slip Angle front-left wheel	β_{11}
	Side-slip Angle front-right wheel	β_{12}
	Side-slip Angle rear-left wheel	β_{21}
	Side-slip Angle rear-right wheel	β_{22}

on the diagonal matrix $\mathbf{R}$ of EKF. The last columns represent the composition of each sensors set: the first is the largest with all measures considered, then the wheels speeds are removed because of their high uncertainty and their not relevant information; after that other measures are gradually removed until getting the last set, that is the smaller and it includes only standard sensors. It is important to remark that even with the largest sensor set, the approach is worth with respect to employ the WFTs.

Table 6.2: Sensors Sets Summary

	Measured Outputs					Sensors Sets				
Ranking	Sensor	Signal	Symbol	Std Dev	Unit	1	2	3	4	5
S	IMU	Roll, Pitch, Yaw rates	$\dot{\phi}\ \dot{\theta}\ \dot{\psi}$	1.628E-1	$^\circ/s$	x	x	x	x	x
		Roll, Pitch, Yaw angles	$\phi\ \theta\ \psi$	1.151E-1	$^\circ$					
		Long., Lat. acc. - CoG	$a_x\ a_y$	4.881E-2	m/s^2					
		Carbody slip angles	$\beta_1\ \beta_2$	1.224E-2	$^\circ$					
S	GPS	GPS pos. - CoG	z_G	2.495E-2	m	x	x	x	x	x
		GPS vel. - CoG	$\dot{x}_G\ \dot{y}_G\ \dot{z}_G$	3.528E-2	m/s					
S	Torque Transducer	Steering torque	T_δ	3.037E-2	Nm	x	x	x	x	
M	DC Gyroscope	Toe, Camber, Self-rotating wheels angles	$\delta_{11}\epsilon_{11}\eta_{11}$ $\delta_{12}\epsilon_{12}\eta_{12}$ $\delta_{21}\epsilon_{21}\eta_{21}$ $\delta_{22}\epsilon_{22}\eta_{22}$	2.809E-2	$^\circ$	x	x	x	x	
M	Optical	Vertical relative suspension displacements	$z_{rel11}z_{rel12}$ $z_{rel21}z_{rel22}$	2.156E-4	m	x	x	x		
A	Optical	Side-slip angles	$\beta_{11}\beta_{12}$ $\beta_{21}\beta_{22}$	1.801E-2	$^\circ$	x	x			
M	Encoder	wheel speeds	$\dot{\theta}_{rel11}\dot{\theta}_{rel12}$ $\dot{\theta}_{rel21}\dot{\theta}_{rel22}$	1.046	$^\circ/s$	x				

Chapter 7

Results

In this chapter, the estimation results of the lateral loads of front and rear axles are reported. For this purpose, the inputs and initialization of the framework have to be defined. As already mentioned, the inputs of the system (estimator model) are the steering wheel angle (δ) and the longitudinal velocity (v_x) (Figure 7.1). The former represents the steering maneuver done by the vehicle, in this case a step-steer maneuver and a sine-steer maneuver are considered; the latter is the velocity imposed to the vehicle in the longitudinal direction and it is considered more or less constant. The two signals considered are not perfect signals, but they are real signals acquired by driving tests, so affected by noise and not with exactly constant amplitude.

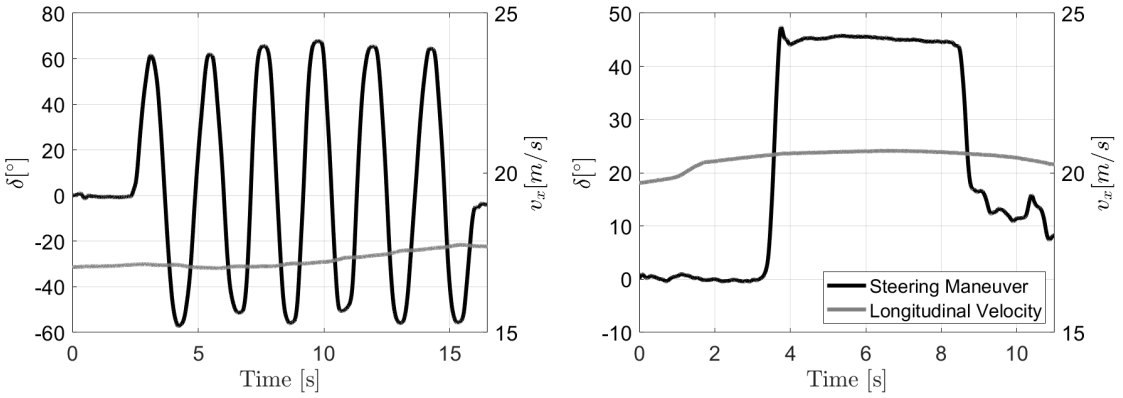

(a) **(b)**

Figure 7.1: Steering maneuver (7.1a sine-steer, 7.1b step-steer) and longitudinal velocity input

Other important quantities to be mentioned are the initialization and matrices of the EKF. In particular the initial state estimate vector $\hat{x}_0$, the process noise

covariance matrix $\mathbf{Q}$, the initial state covariance matrix P_0 and the measurement noise covariance matrix $\mathbf{R}$. The components of $\hat{x}_0$ are taken from simulation models, $\mathbf{Q}$ is a diagonal matrix and all the uncertainty is on the cornering stiffnesses that due to the linear adaptive tyre model are the most critical parameters and finally P_0 is matrix of zeros because the initial state vector is not affected by uncertainty. All the above specified quantities are present in Table 7.1. $\mathbf{R}$ is a diagonal matrix as well and the diagonal elements are the values of standard deviation present in Table 6.2 squared.

Before showing the estimation results it is important to consider the observability analysis conducted on the system, having an overview of the methods used and some mentions on the projection approach for this system.

Table 7.1: Initialization state vector, square root of diagonal elements of state covariance matrix and process noise covariance matrix

State	x_0	$\sqrt{\mathbf{Q}_{ii}}$	$\sqrt{P_{0_{ii}}}$	Unit
$\dot{x}_G$	17	0	0	m/s
$\dot{y}_G$	0	0	0	m/s
$\dot{z}_G$	0	0	0	m/s
z_G	0.38	0	0	m
$\dot{\phi}$	0	0	0	$^\circ/s$
$\dot{\theta}$	0	0	0	$^\circ/s$
$\dot{\psi}$	0	0	0	$^\circ/s$
ϕ	0	0	0	$^\circ$
θ	0	0	0	$^\circ$
ψ	0	0	0	$^\circ$
$\dot{z}_{rel11}$	0	0	0	m/s
z_{rel11}	0	0	0	m
$\dot{\theta}_{rel11}$	3264.76	0	0	$^\circ/s$
$\dot{z}_{rel12}$	0	0	0	m/s
z_{rel12}	0	0	0	m
$\dot{\theta}_{rel12}$	3264.76	0	0	$^\circ/s$
$\dot{z}_{rel21}$	0	0	0	m/s
z_{rel21}	0	0	0	m
$\dot{\theta}_{rel21}$	3264.76	0	0	$^\circ/s$
$\dot{z}_{rel22}$	0	0	0	m/s
z_{rel22}	0	0	0	m
$\dot{\theta}_{rel22}$	3264.76	0	0	$^\circ/s$
C_{yF}	660	0.1	0	$N/^\circ$
C_{yR}	910	0.1	0	$N/^\circ$

7.1 Observability Results

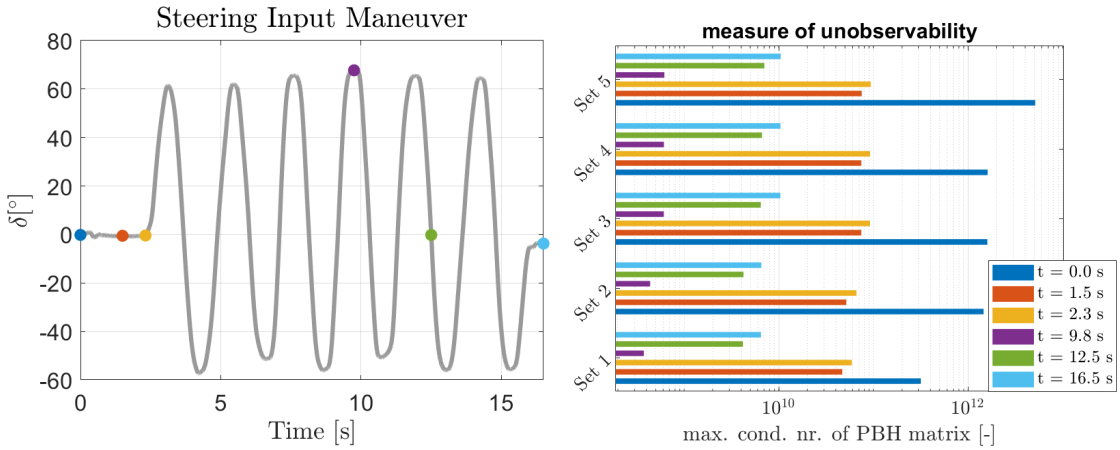

(a) **(b)**

Figure 7.2: PBH analysis: 7.2a is the sine-steer input meneuver with the markers in the specific times in which PBHs are computed, 7.2b shows the condition numbers of PBH matrices for all the sets and for different times

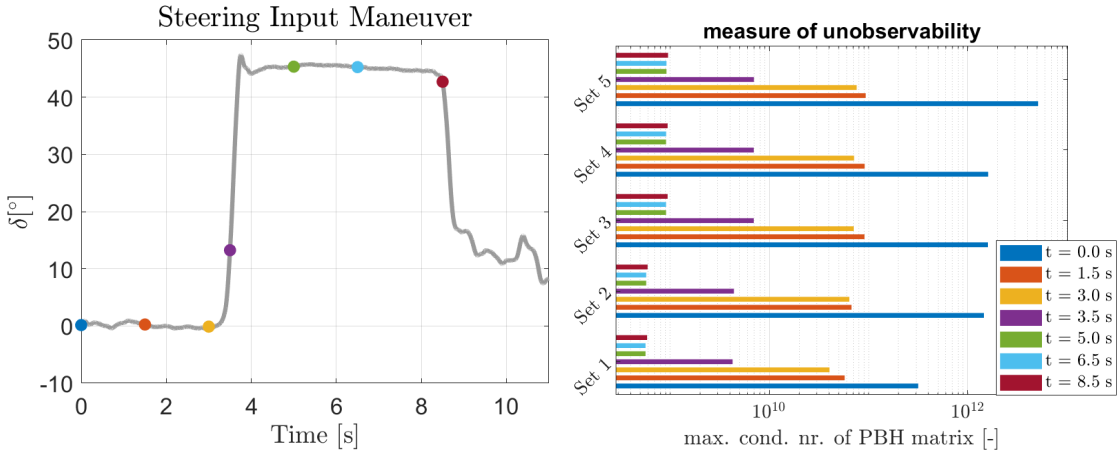

(a) **(b)**

Figure 7.3: PBH analysis: 7.3a is the step-steer input meneuver with the markers in the specific times in which PBHs are computed, 7.3b shows the condition numbers of PBH matrices for all the sets and for different times

The first is the PBH test. It is conducted considering two inputs: the sine-steer (Figure 7.2) and the step-steer (7.3) maneuvers. It is important to remark then

that every observability analysis does not depend from the type of input, but it can be useful to show some results. Plotting the condition numbers, shows how much a system is observable (or not) in a specific time instant and considering a specific sensor set. It is clear that the observability decreases (condition numbers increase) from sensor set 1 to sensor set 5 because the system looses information. Another important aspect is that the system has a lack of observability when the vehicle goes straight, while during the maneuver the system is observable. Intuitively the unobservable states could be the cornering stiffnesses because, when the car drives in a straight line, the wheels slip angles and the lateral forces are equal to zero and looking at the relations (4.1) and (4.4), it is clear that the cornering stiffnesses cannot be determined. Moving to the analysis of the total observability matrix through SVD, in Figures from 7.4 to 7.8, the singular values of every total observability matrix, computed considering different sensors sets and the components of the singular vectors that belong to the unobservable subspace. Looking at Figure 7.4, it is visible a little gap before the last two singular values and the corresponding singular vectors present the components related to the cornering stiffnesses different from zero. Considering the other sensors sets it seems that the size of the unobservable space is six and the states affected by unobservability are the cornering stiffnesses and the relative wheels speeds as well. The other two analysis tools, The FIM and sensitivity indices, are not available for this system. The former is not possible to compute because of some numerical issues in propagating the FIM and also due to the initialization of FIM that is defined as the inverse of P_0 that in this case, for a matter of stability of EKF algorithm, is a matrix of zeros; the latter is a tool that is strongly depending on normalization. Due to complexity and difference between quantities involved in states and measurements, the normalization or scaling matrices change the results and the ranking of the sensors, so the sensitivity indices result as not trustworthy indicators.

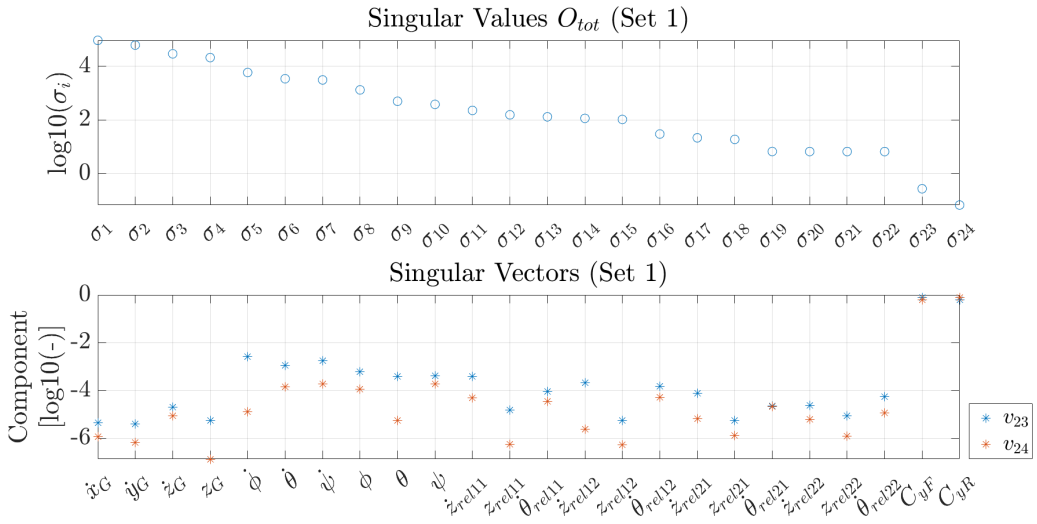

Figure 7.4: Singular Values (σ_i) of total obsevability matrix O_{tot} and components of singular vectors belonging to the unobservable subspace, considering sensors set 1 (on the x-axis of singular vectors plot the referring states are reported)

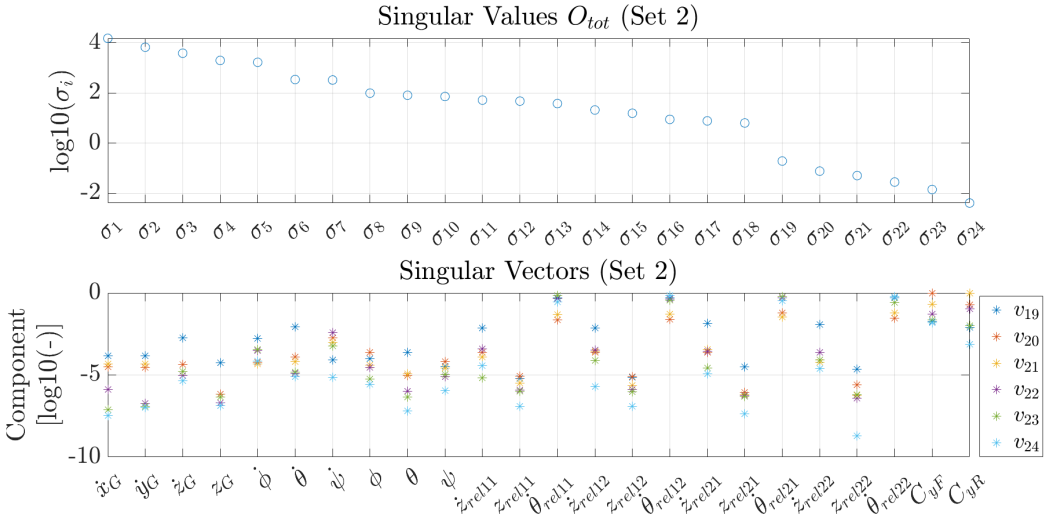

Figure 7.5: Singular Values (σ_i) of total obsevability matrix O_{tot} and components of singular vectors belonging to the unobservable subspace, considering sensors set 2 (on the x-axis of singular vectors plot the referring states are reported)

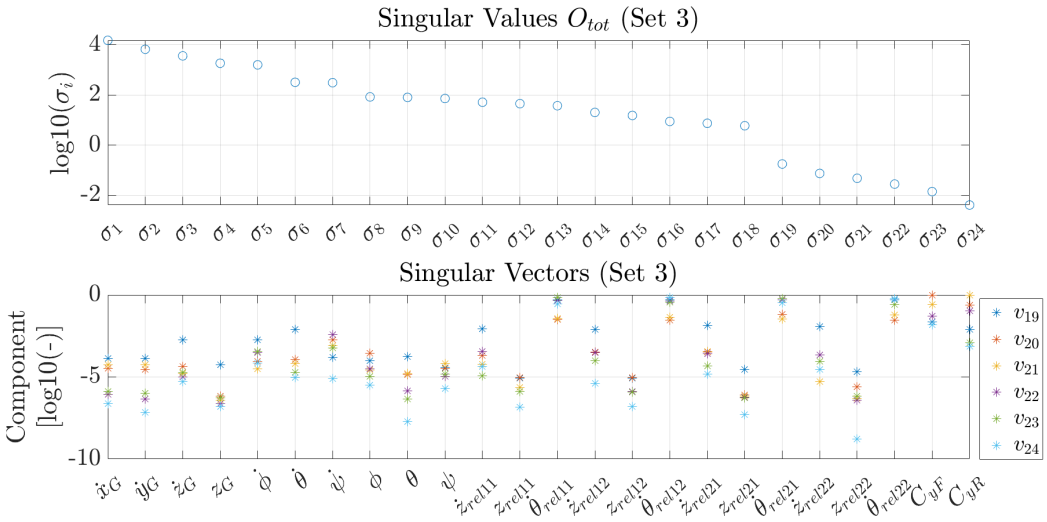

Figure 7.6: Singular Values (σ_i) of total obsevability matrix O_{tot} and components of singular vectors belonging to the unobservable subspace, considering sensors set 3 (on the x-axis of singular vectors plot the referring states are reported)

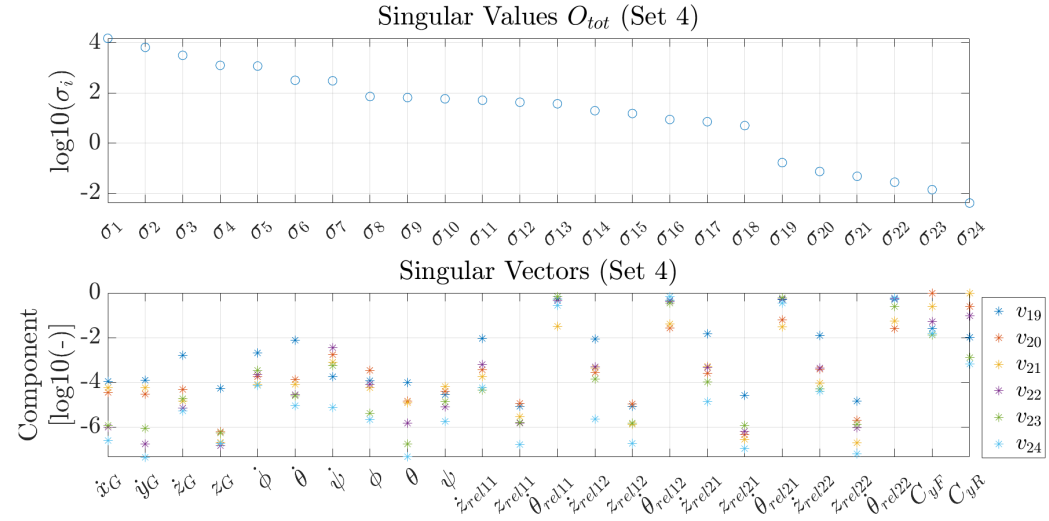

Figure 7.7: Singular Values (σ_i) of total obsevability matrix O_{tot} and components of singular vectors belonging to the unobservable subspace, considering sensors set 4 (on the x-axis of singular vectors plot the referring states are reported)

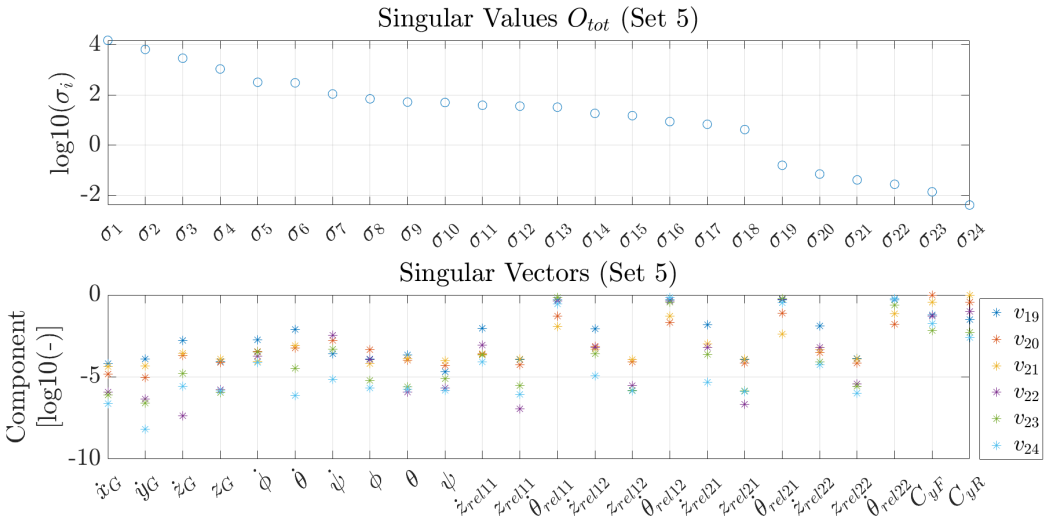

Figure 7.8: Singular Values (σ_i) of total obsevability matrix O_{tot} and components of singular vectors belonging to the unobservable subspace, considering sensors set 5 (on the x-axis of singular vectors plot the referring states are reported)

Taking the Figure 7.4, the gap between singular values is not so clear, so it cannot be proved a priori the advantage in using the projection approach. In order to go into details, a local analysis is performed. The singular values evolution in time is plotted for a sine-steer (Figure 7.9a) and step-steer (Figure 7.9a) input. They have been computed considering the SVD of the observability matrices of all the time instants. It is clear that there is a gap, more marked at the beginning (the vehicle goes straight). The idea is to consider a local projection basis: every time instant (or every some time instant) the local observability matrix is computed and, according to number of the singular values that are lower than a certain threshold, the EKF is projected into the observable subspace. The problem is in choosing the threshold: considering the Threshold 1, it means basically apply the entire projection approach, but in this case, since all the uncertainty is on the cornering stiffnesses, it basically means doing a pure simulation of the system; considering the Threshold 2 allows in principle to overcome the unobservability of the first part, but actually the crossing points introduce in the estimation algorithm lots of shocks. In Figure 7.10 the variance propagation of cornering stiffnesses (without any projection) is depicted and it is clear that the algorithm is stable in any case because after rising, the variances become stable during the maneuver.

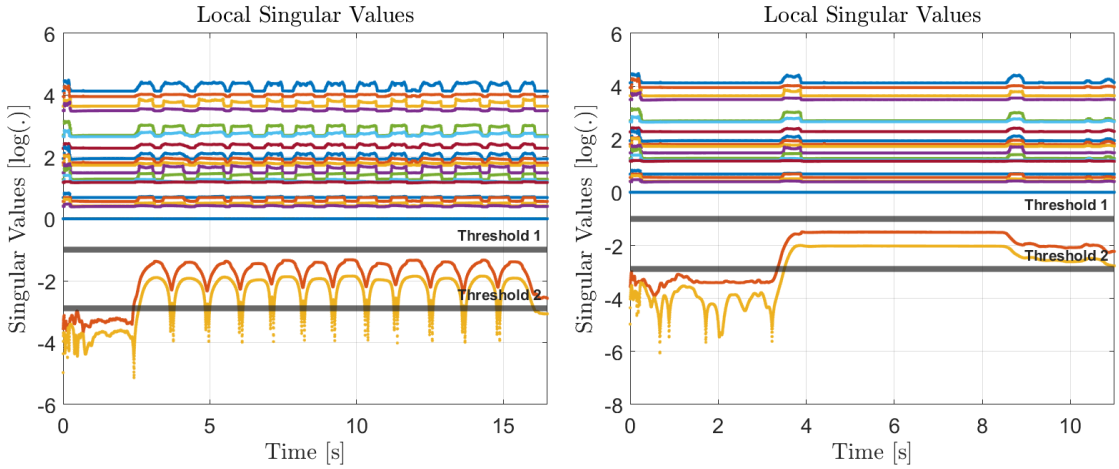

(a) (b)

Figure 7.9: Local singular values evolution in time

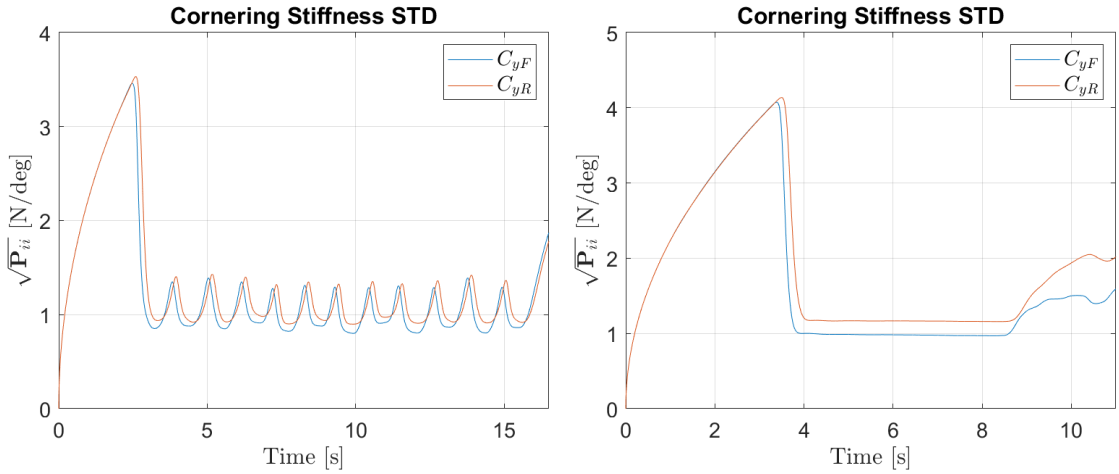

(a) (b)

Figure 7.10: Local singular values evolution in time

7.2 Estimation Results

In this chapter the estimation results regarding the lateral loads of front and rear axles are presented. The lateral loads are computed as sum of individual load as follows:

$$\mathbf{F}_1 = \mathbf{F}_{11} + \mathbf{F}_{12} \qquad \mathbf{F}_2 = \mathbf{F}_{21} + \mathbf{F}_{22} \tag{7.1}$$

There is is no need to project and sum the longitudinal force contribution because the lateral and longitudinal forces can be considered decoupled due to the small steering and side-sleep angles.

In the work only the estimation results considering a step-steer maneuver are reported because the transient and build-up section of the force is more visible. The main focus of this work is the accuracy of the lateral loads during the build-up phase because, due to the dynamics, it is the most difficult part in which obtaining a good estimation and, moreover, it is the discriminant part to decide if the virtual sensing approach with 15DoFs model can lead to effective advantage with respect to WFTs. The same approach with the single track model led to errors in time, during the build-up phase, up to 30 ms that is too much.

7.2.1 Front Axle Load

The estimated front axle loads are plotted comparing the reference forces, coming from the simulated reference models, with the estimation results obtained considering the different sensors sets (Figures from 7.11 to 7.15). It is important to note that, during the transient, the errors over time, even in the worst case, are less than 10-15 ms, so this approach results in having more than halved the errors compared to the bicycle model. The framework results to be quite robust with respect to the presence of modelling errors (Figures 7.12, 7.13, 7.14). As expected there is a loss of accuracy considering the reference model with elastokinematics (Figure 7.15), because it introduces difficult dynamics. For all the estimations, the last three sensors sets (set 3,4,5) give quite the same results, so there is not a great advantage in using a more complex set (such as set 3) with respect to a smaller one (set 5). It is important to notice that before $t \simeq 3.52s$, the estimated loads are indistinguishable, after that for sensors sets 1 and 2, the signals top the reference, while for the other sets, the estimated loads are lower.

7.2.2 Rear Axle Load

The estimated rear axle loads are plotted comparing the reference forces, coming from the simulated reference models, with the estimation results obtained considering the different sensors sets (Figures from 7.16 to 7.20). In this case, the results are less accurate with respect to the front axle. It happens because commonly the errors propagates from the front axle, where there is the steering action, to the rear one, accumulating and affecting the estimation quality. It is also clear from the fact that the estimated signals, for every sensors sets, over-estimate the reference.

7.2.3 Tuning Effect

In order to overcome the errors accumulation in rear axle, a solution could be trying to tune the EKF. Tuning the EKF means making action on **Q** and **R** matrices in order to obtain better results. In this case it is clear that the main parameter to change is the uncertainty of the rear cornering stiffness (in **Q** matrix). Increasing this uncertainty, it allows the the rear cornering stiffness to better adapt to the system dynamics, mitigating the errors propagation. Taking into account two sensors sets, the tuning effect on estimation results is shown in Figures from 7.21 to 7.30. The set 2 is one of the most complete, giving a large quantity of information, thus there is no need to tune the front axle cornering stiffness uncertainty, because the estimation is already accurate, while increasing the rear cornering stiffness uncertainty lead to a surprising better results in rear forces estimation. It is interesting looking at the effect that tuning has on the estimation with sensor set 5. It is the simplest set, which contains only standard measures. Tuning both front and rear cornering stiffness uncertainties, the results in estimation are promising, considering in fact the simplicity of the set used. The most significant result is depicted in Figure 7.30, where the loads estimated with tuning can catch the complex dynamics introduced by elatokinematics with no great differences (in transient) between the two sensors sets used.

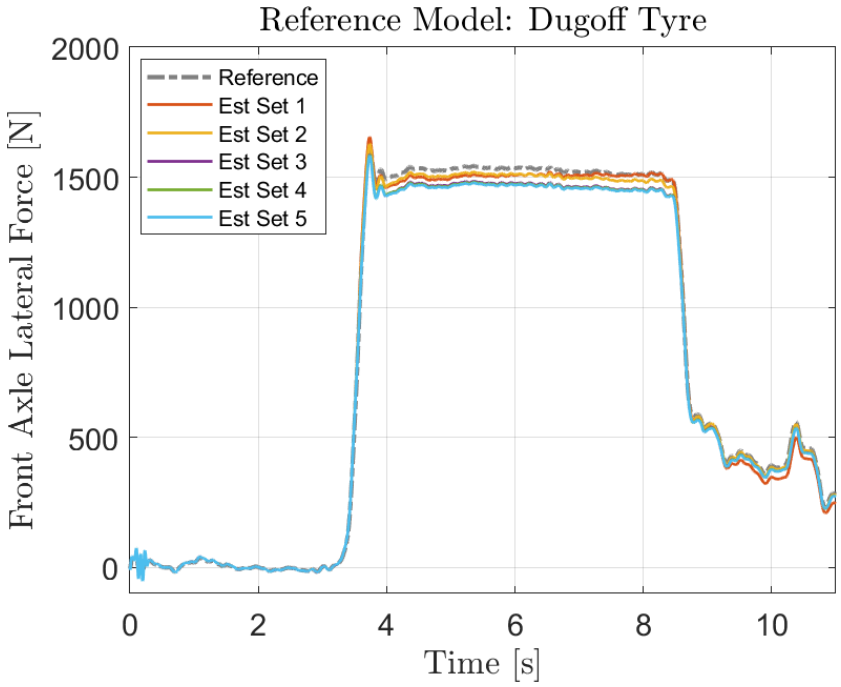

(a)

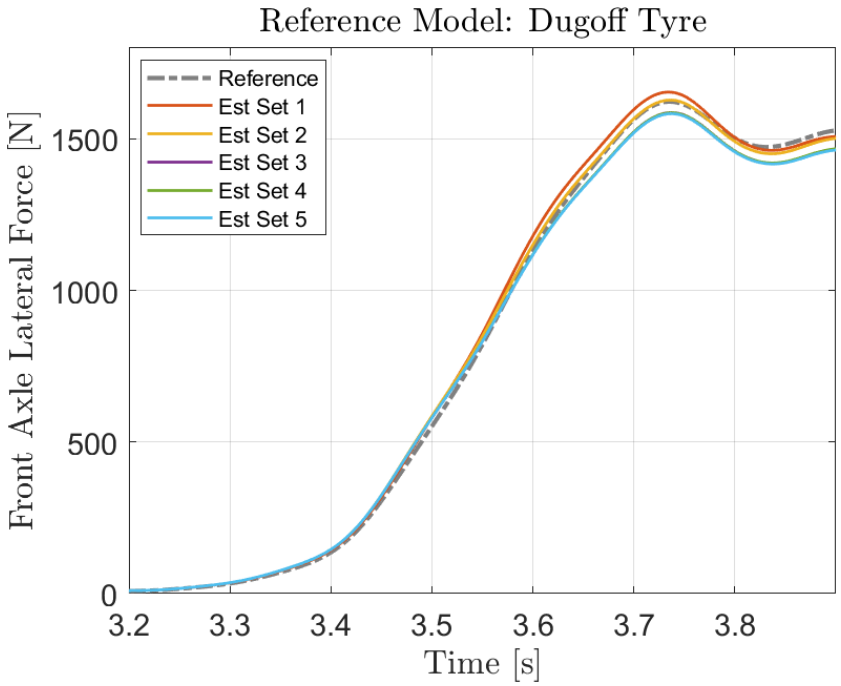

(b) Build-up zoom

Figure 7.11: Front Axle Load Estimation. Dugoff tyre reference model

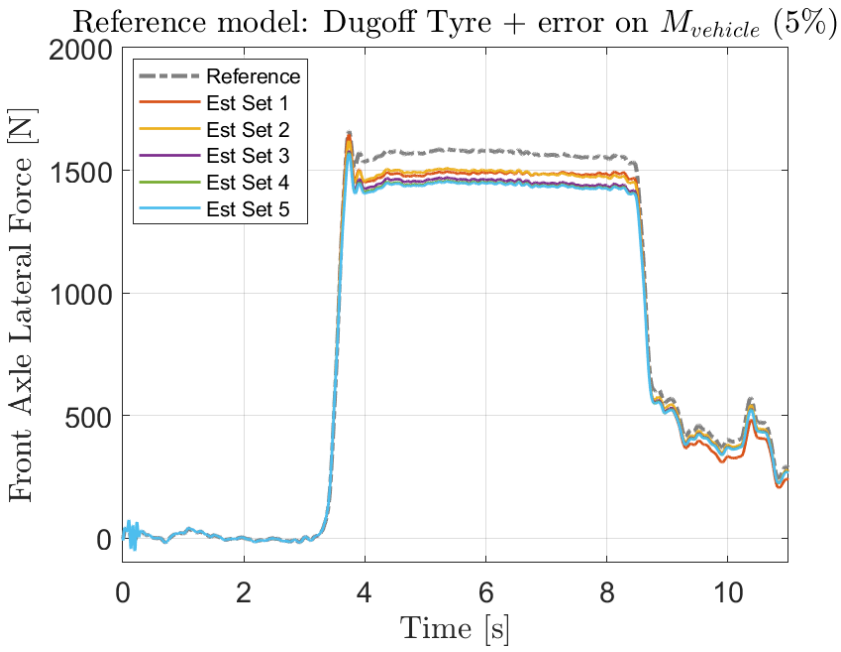

(a)

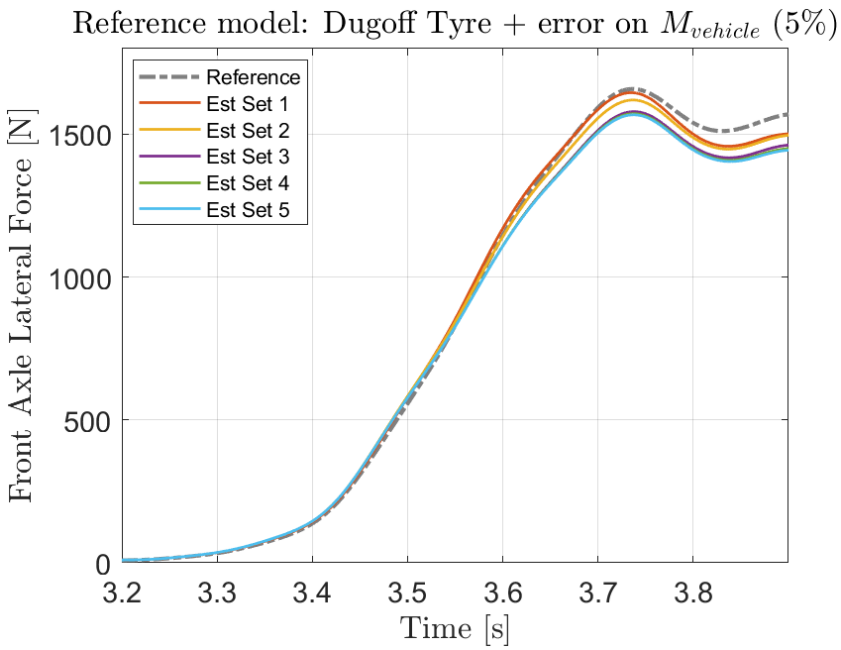

(b) Build-up zoom

Figure 7.12: Front Axle Load Estimation. Dugoff tyre reference model + error on car mass

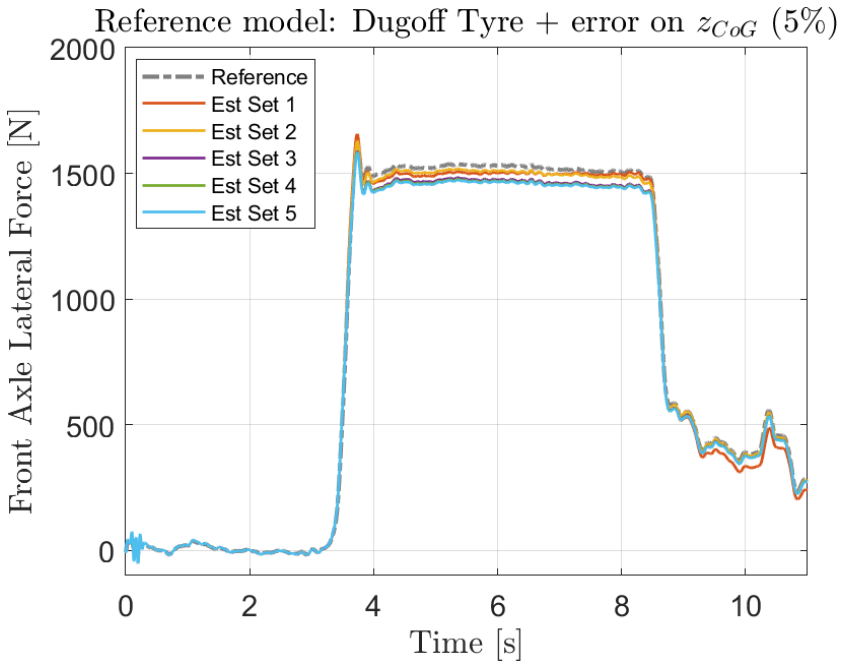

(a)

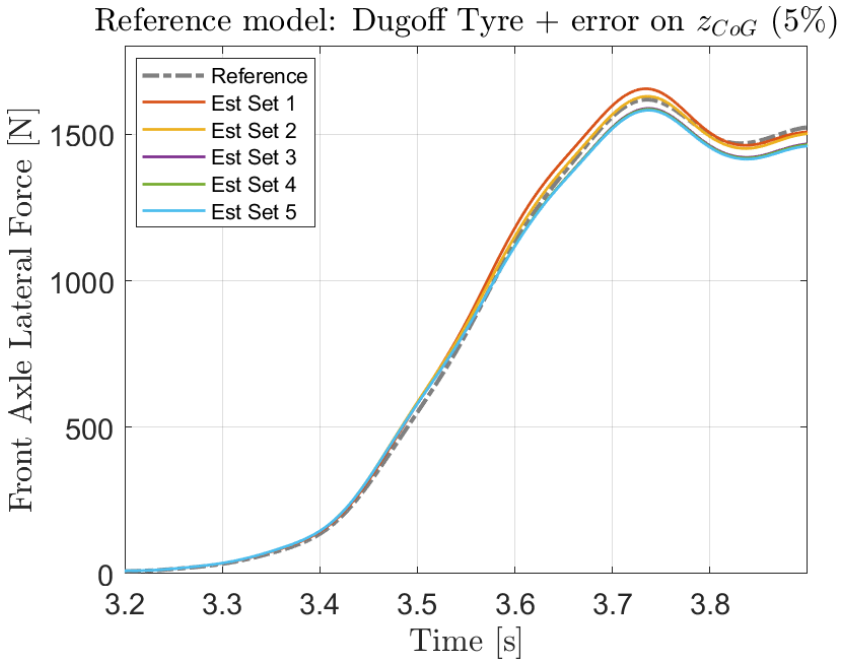

(b) Build-up zoom

Figure 7.13: Front Axle Load Estimation. Dugoff tyre reference model + error on CoG heigh

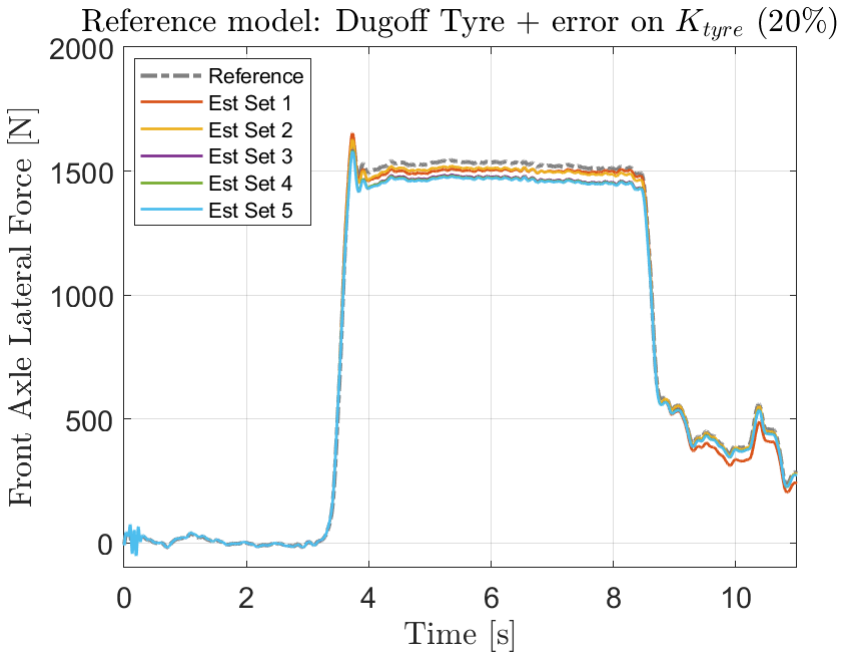

(a)

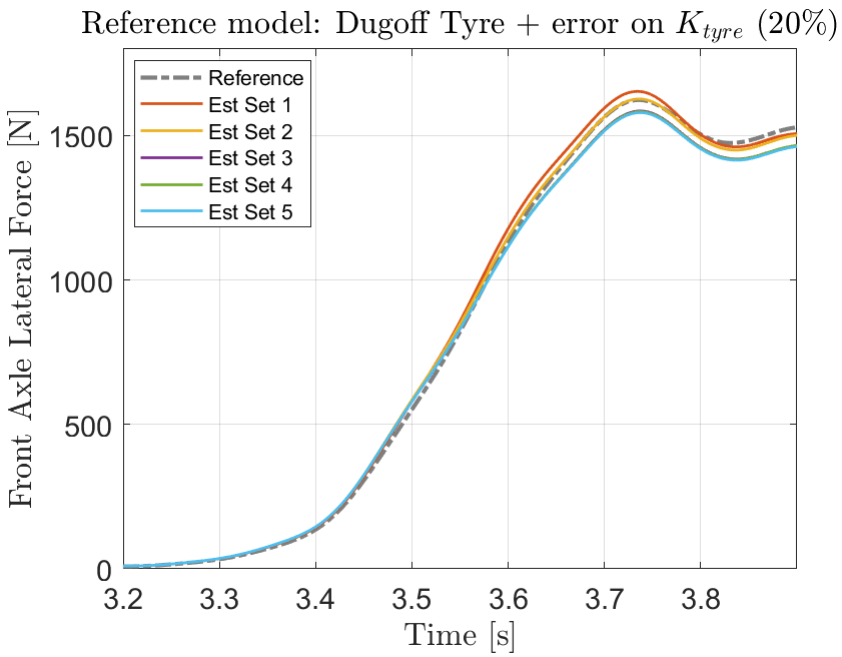

(b) Build-up zoom

Figure 7.14: Front Axle Load Estimation. Dugoff tyre reference model + error on tyre stiffness

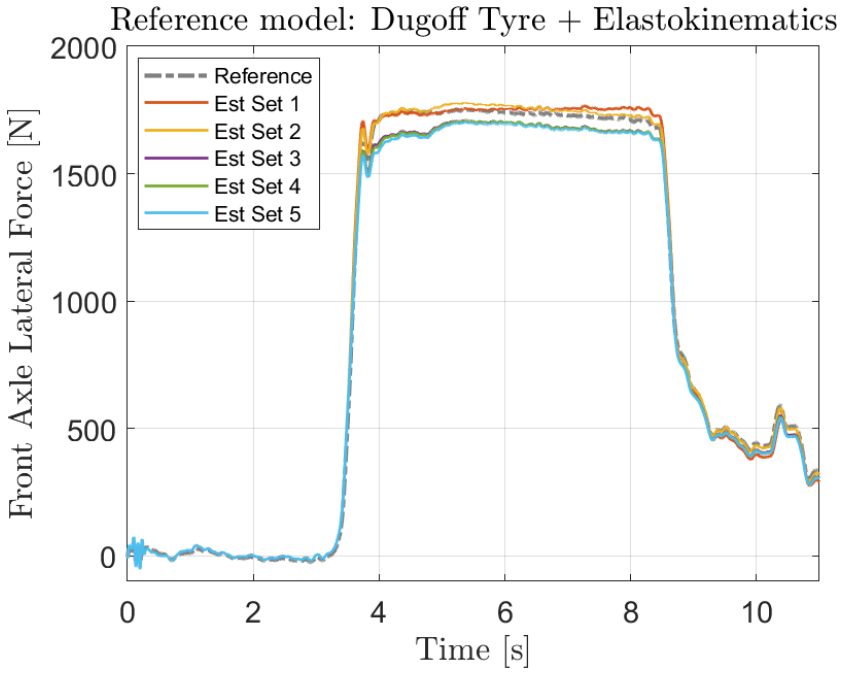

(a)

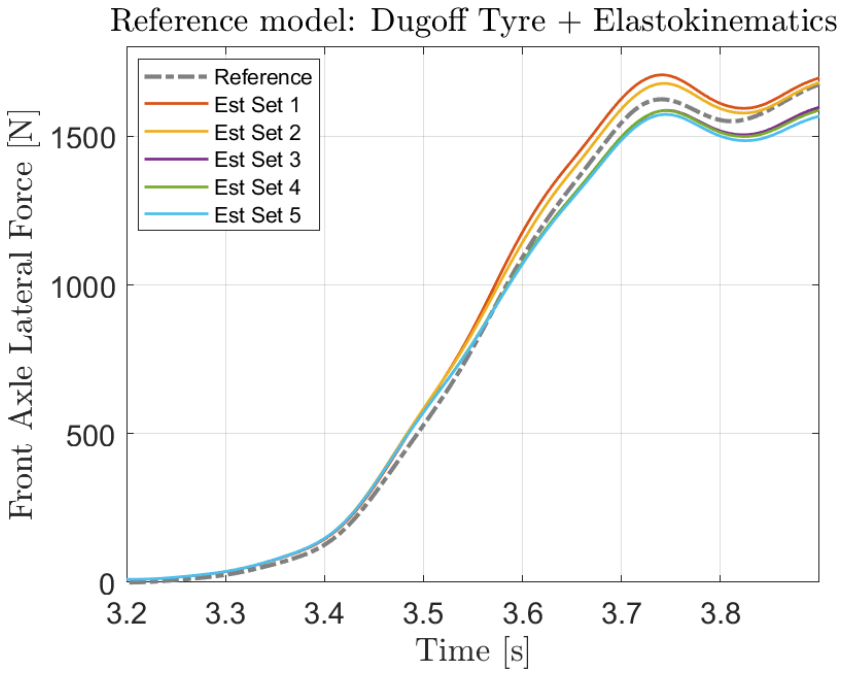

(b) Build-up zoom

Figure 7.15: Front Axle Load Estimation. Dugoff tyre reference model + elastokinematics

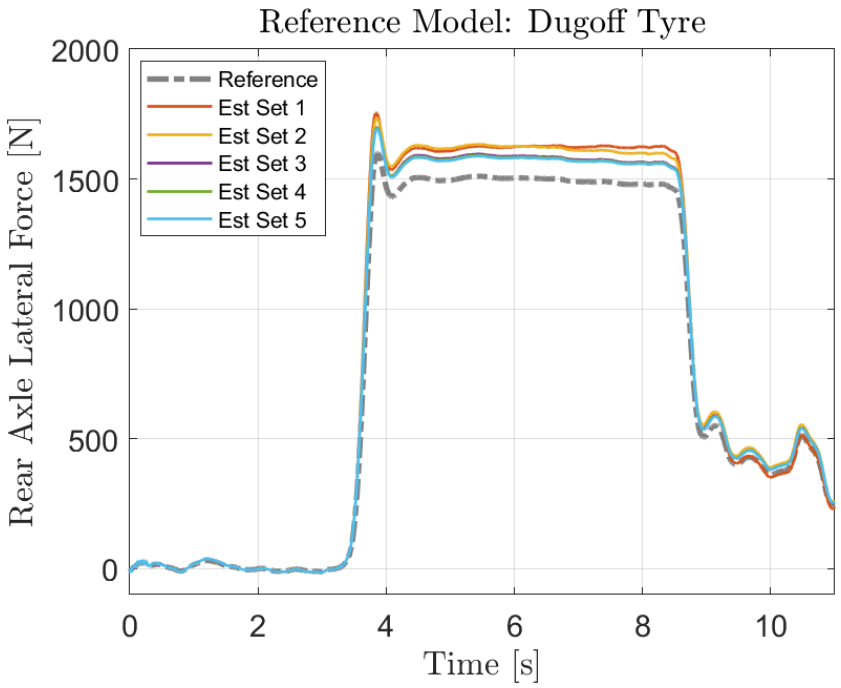

(a)

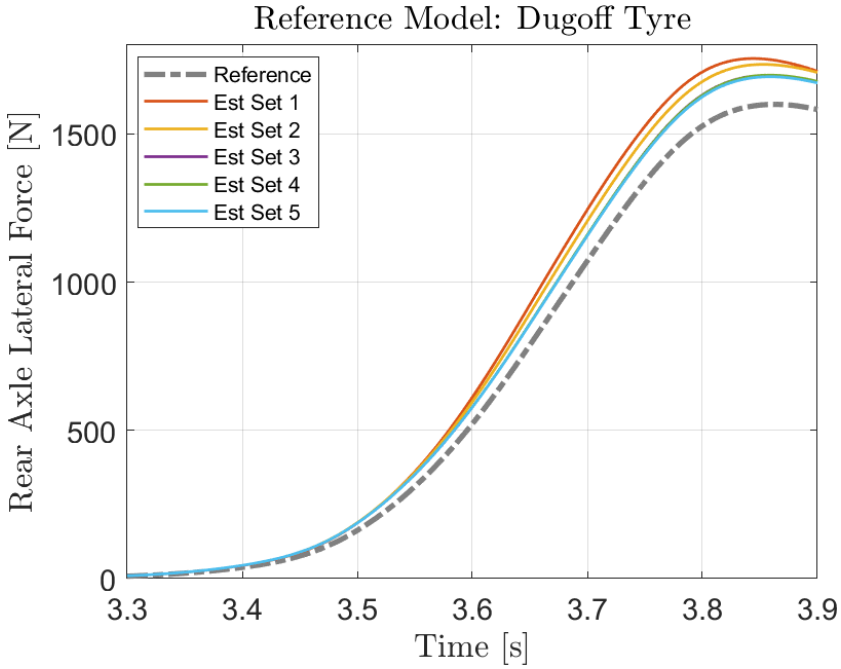

(b) Build-up zoom

Figure 7.16: Rear Axle Load Estimation. Dugoff tyre reference model

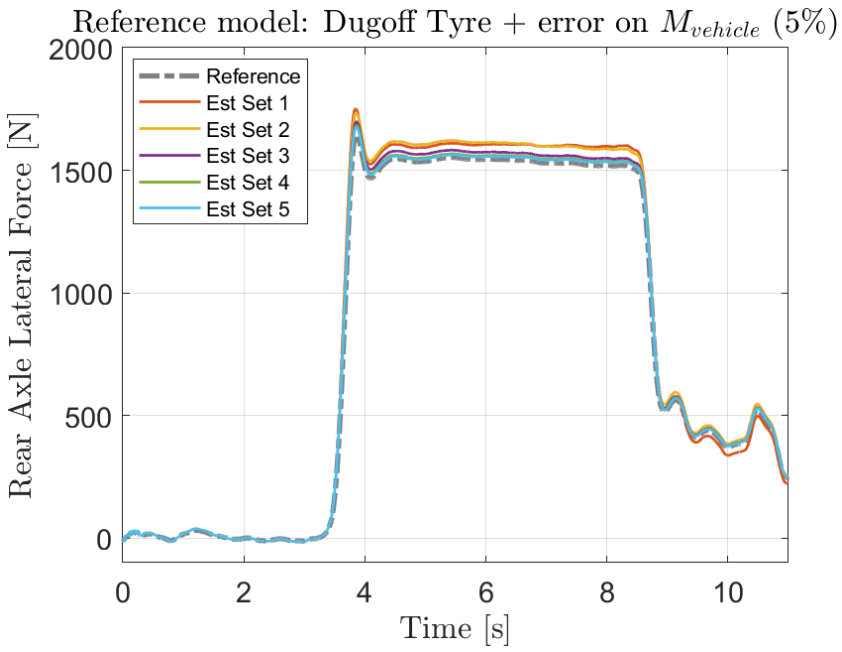

(a)

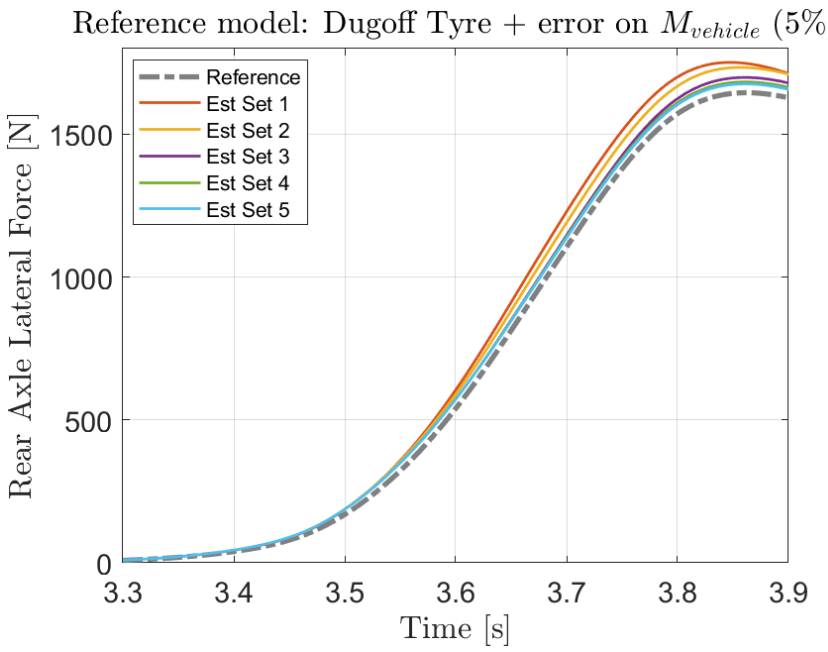

(b) Build-up zoom

Figure 7.17: Rear Axle Load Estimation. Dugoff tyre reference model + error on car mass

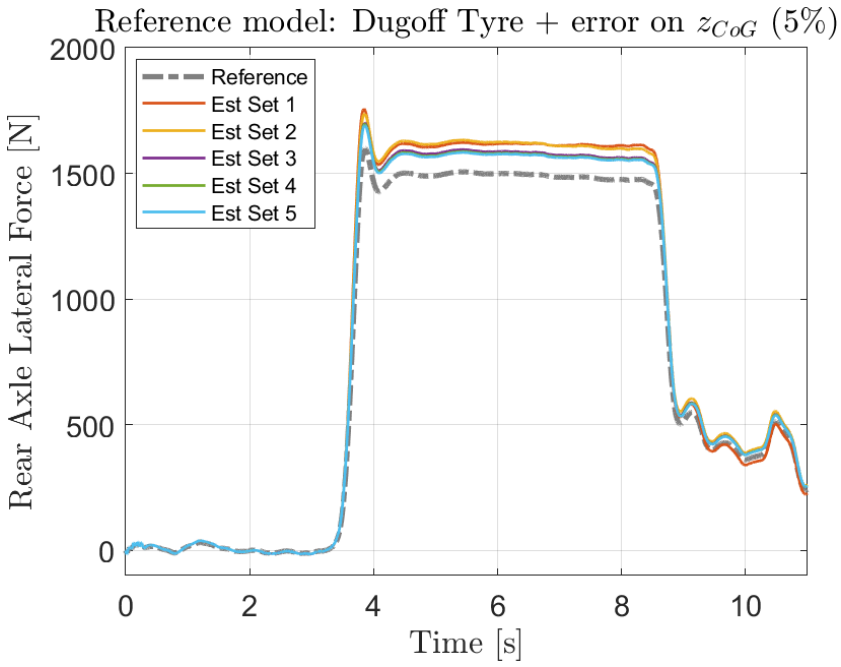

(a)

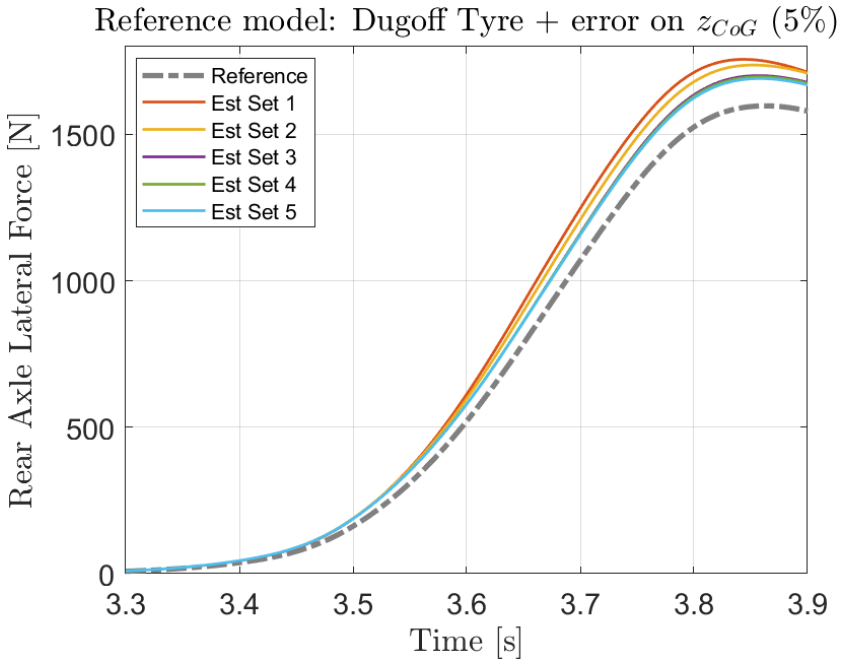

(b) Build-up zoom

Figure 7.18: Rear Axle Load Estimation. Dugoff tyre reference model + error on CoG heigh

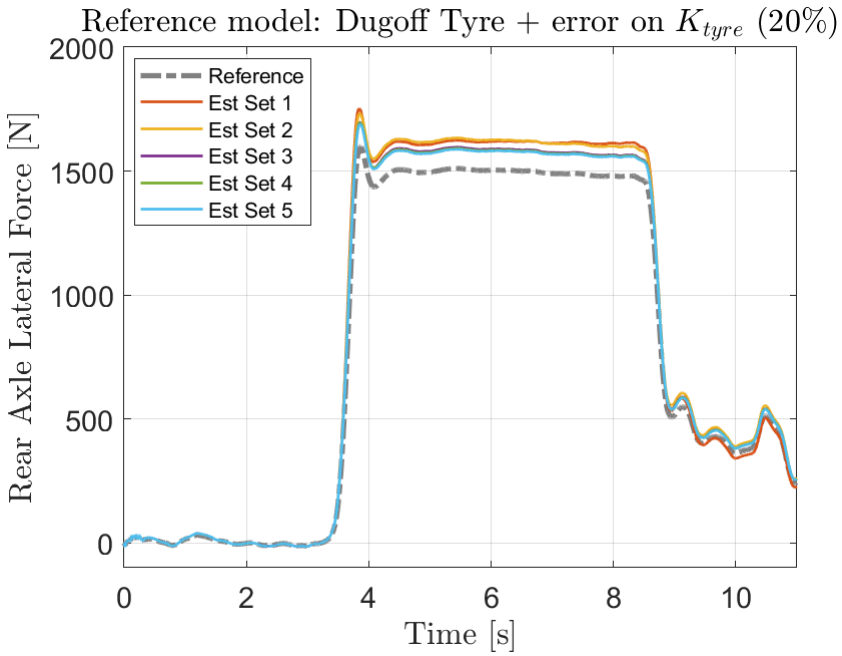

(a)

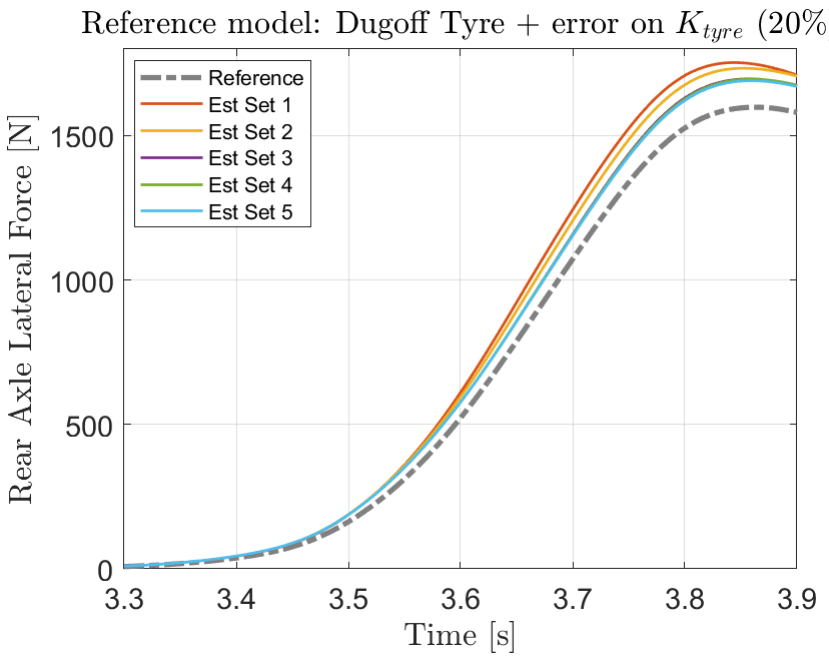

(b) Build-up zoom

Figure 7.19: Rear Axle Load Estimation. Dugoff tyre reference model + error on tyre stiffness

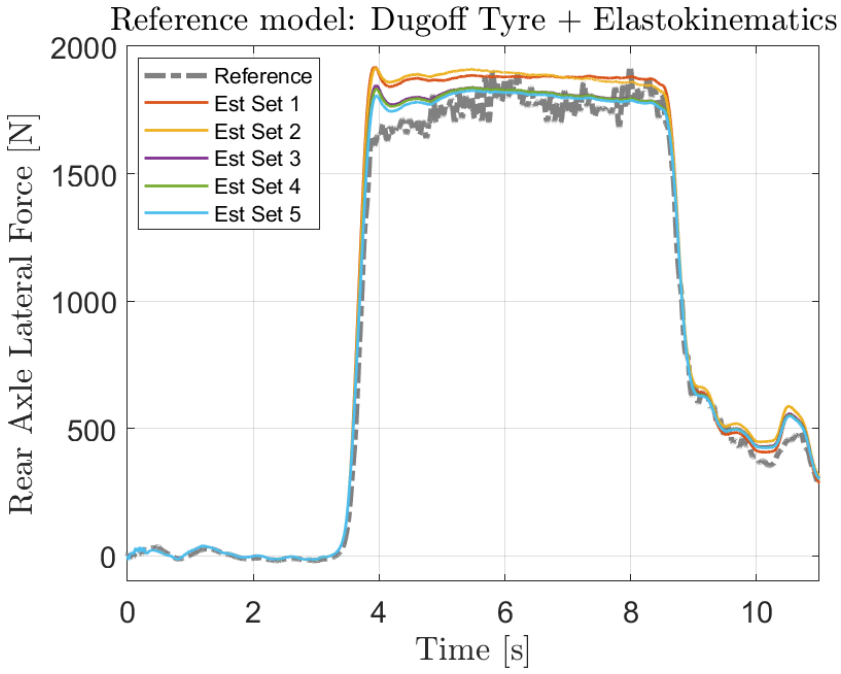

(a)

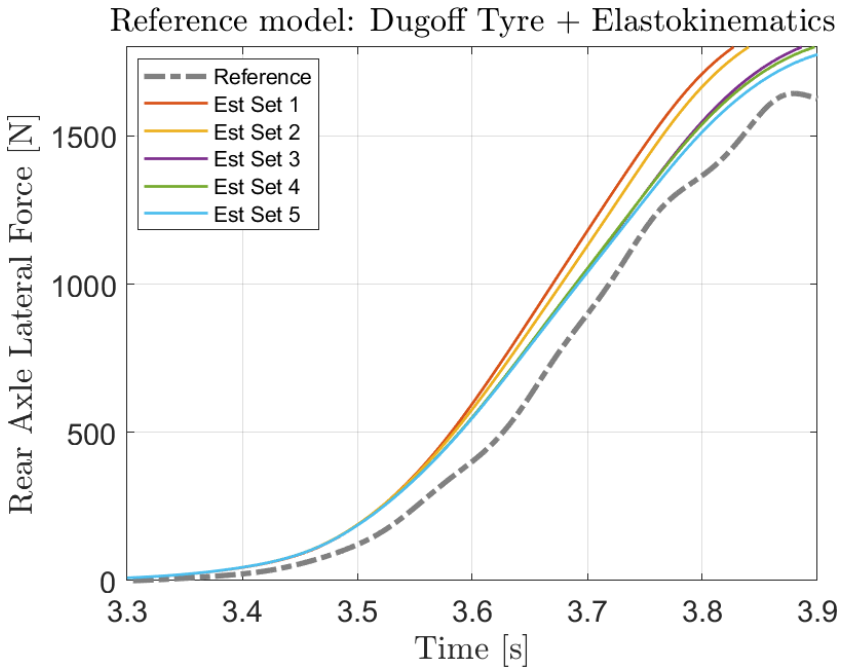

(b) Build-up zoom

Figure 7.20: Rear Axle Load Estimation. Dugoff tyre reference model + elastokinematics

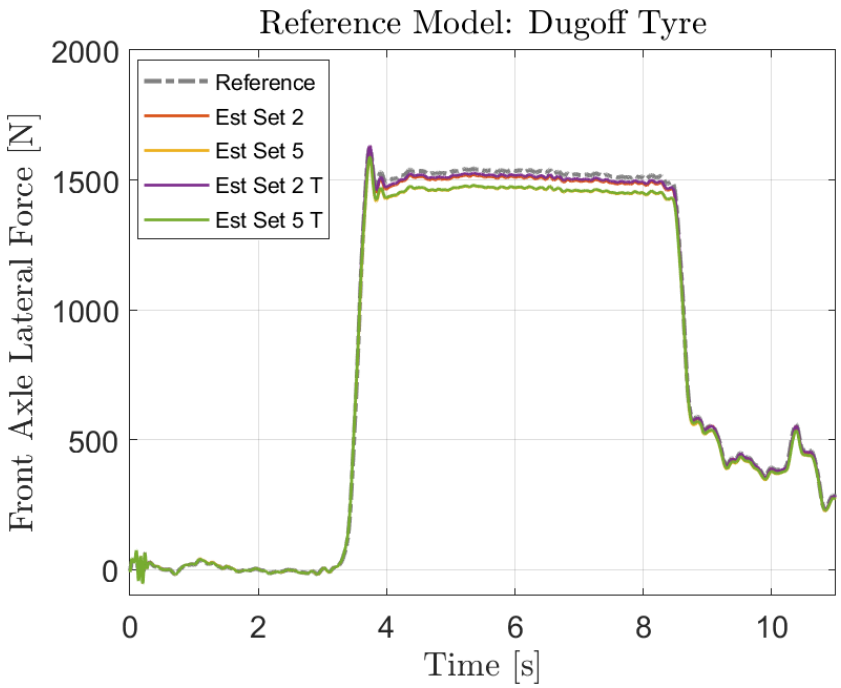

(a)

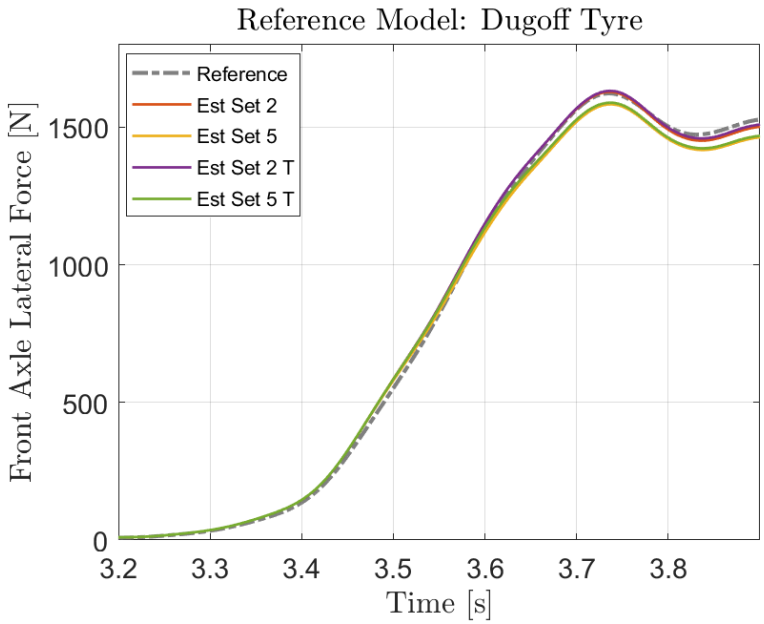

(b) Build-up zoom

Figure 7.21: Front Axle Load Estimation Tuned. Dugoff tyre reference model

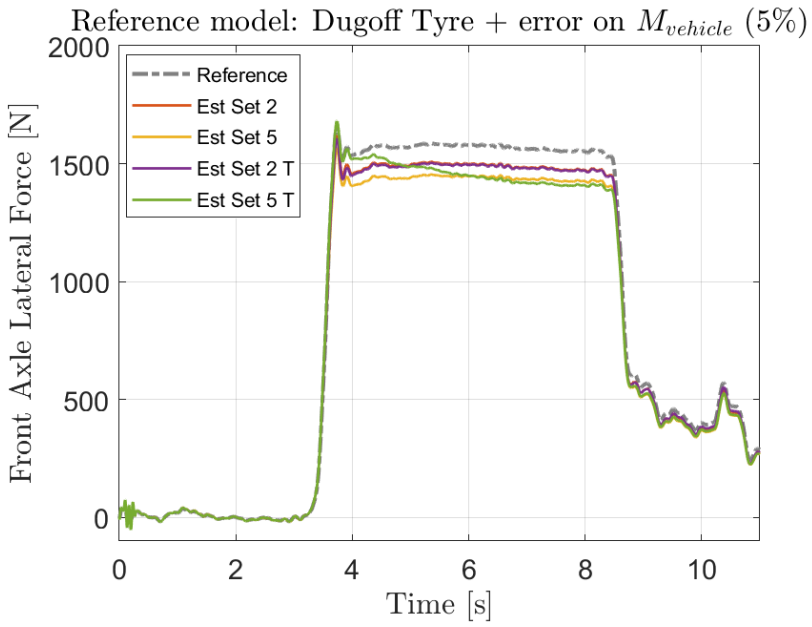

(a)

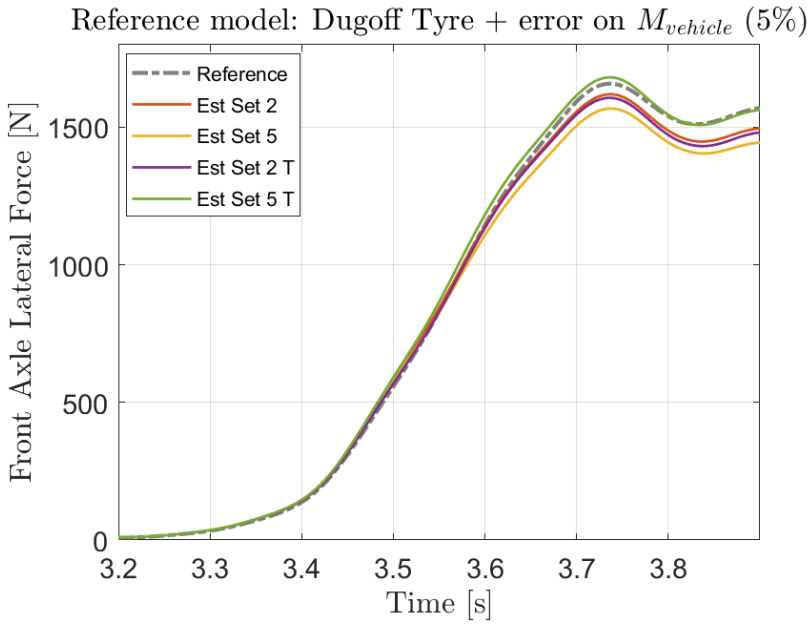

(b) Build-up zoom

Figure 7.22: Front Axle Load Estimation Tuned. Dugoff tyre reference model + error on car mass

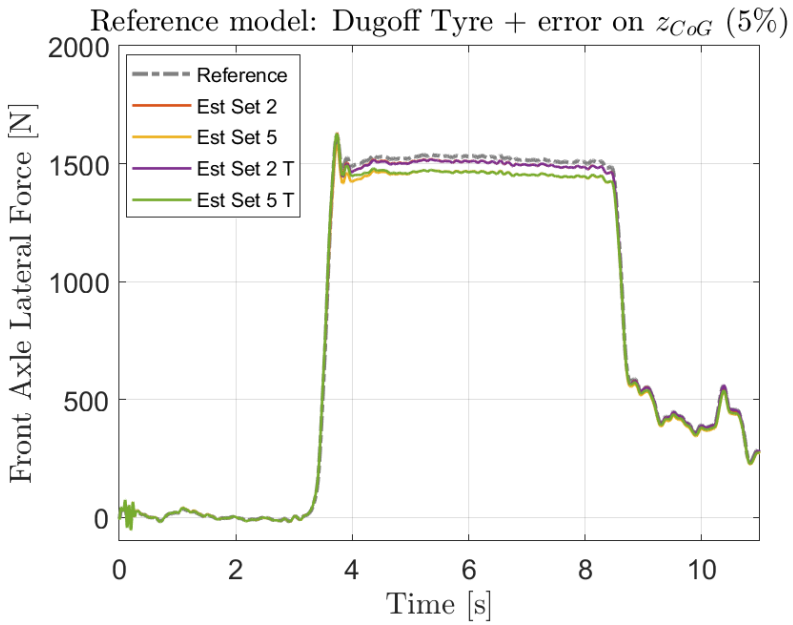

(a)

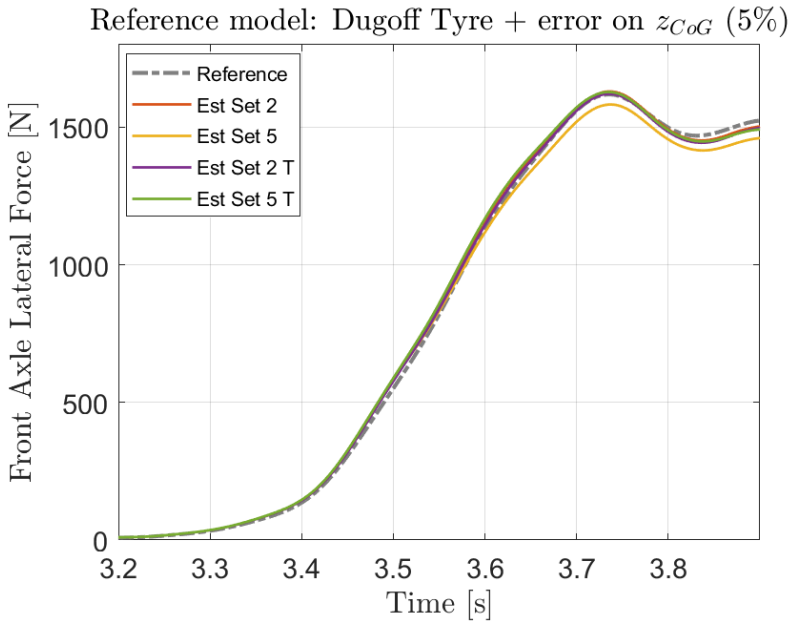

(b) Build-up zoom

Figure 7.23: Front Axle Load Estimation Tuned. Dugoff tyre reference model + error on CoG heigh

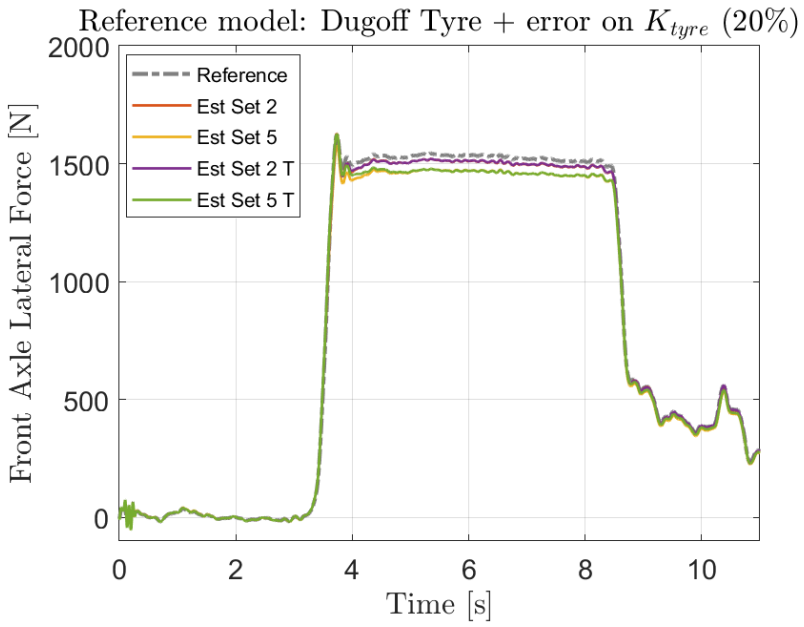

(a)

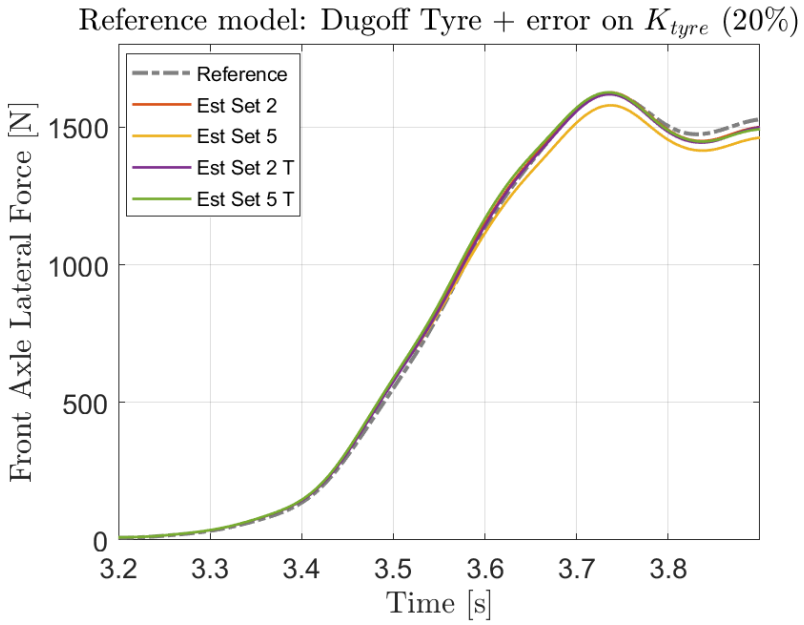

(b) Build-up zoom

Figure 7.24: Front Axle Load Estimation Tuned. Dugoff tyre reference model + error on tyre stiffness

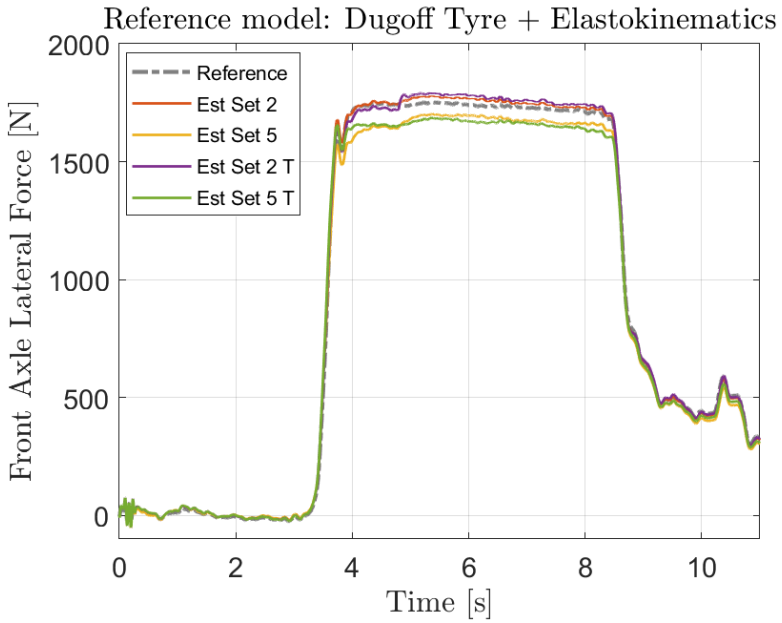

(a)

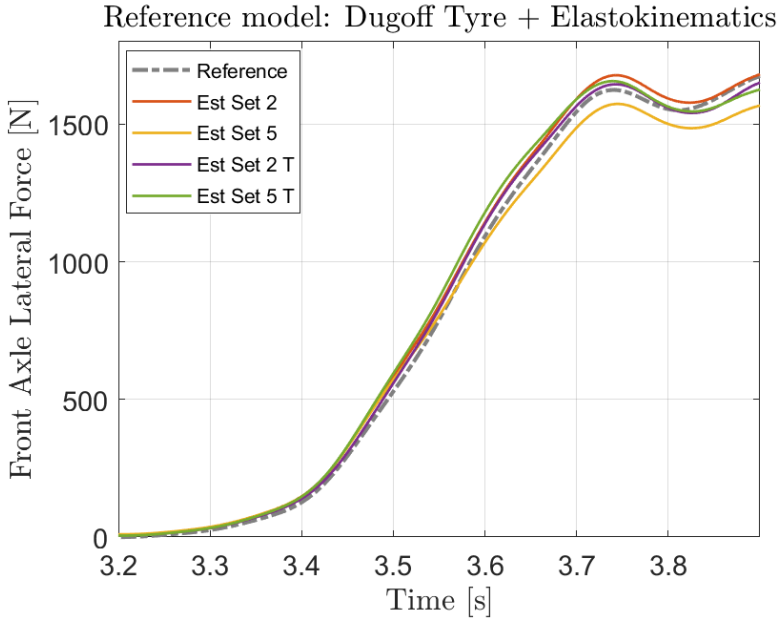

(b) Build-up zoom

Figure 7.25: Front Axle Load Estimation Tuned. Dugoff tyre reference model + elastokinematics

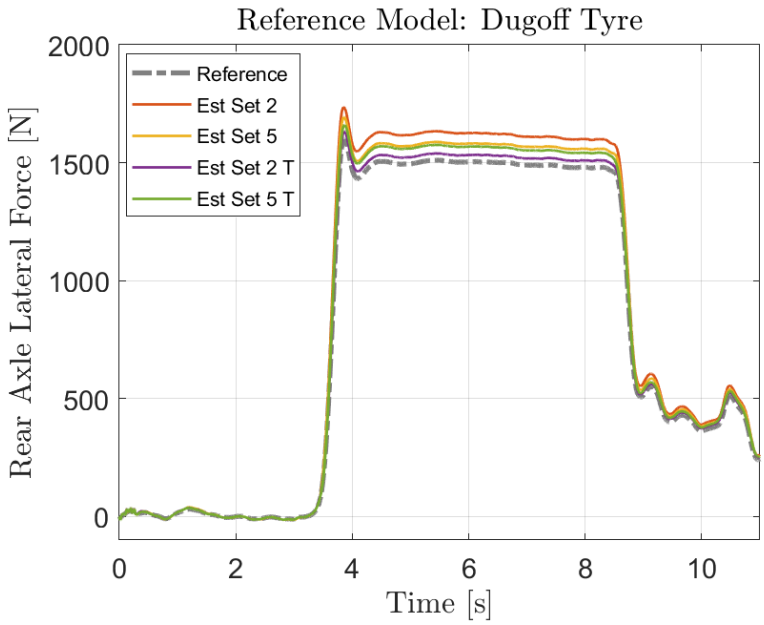

(a)

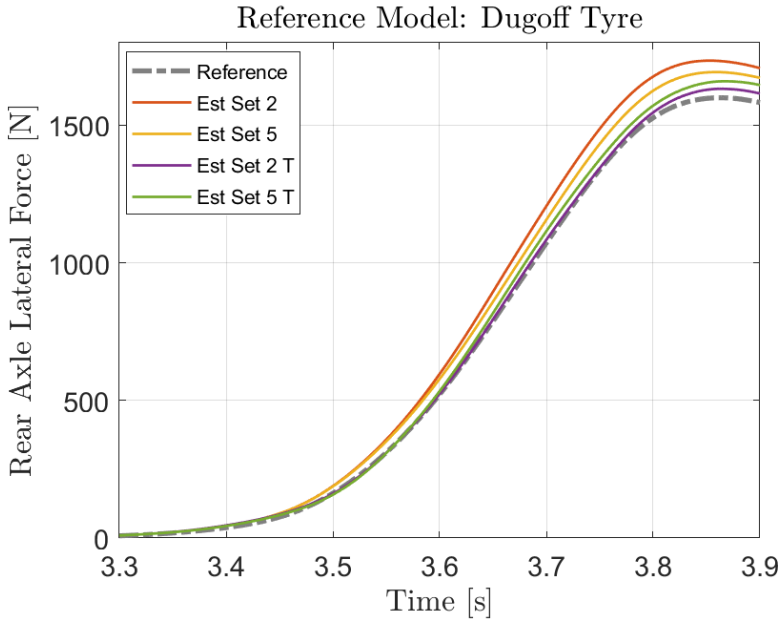

(b) Build-up zoom

Figure 7.26: Rear Axle Load Estimation Tuned. Dugoff tyre reference model

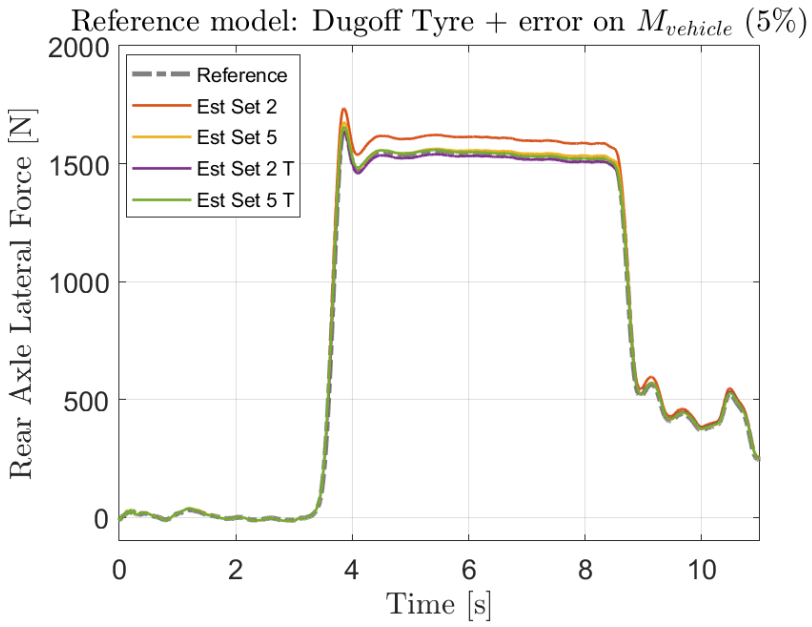

(a)

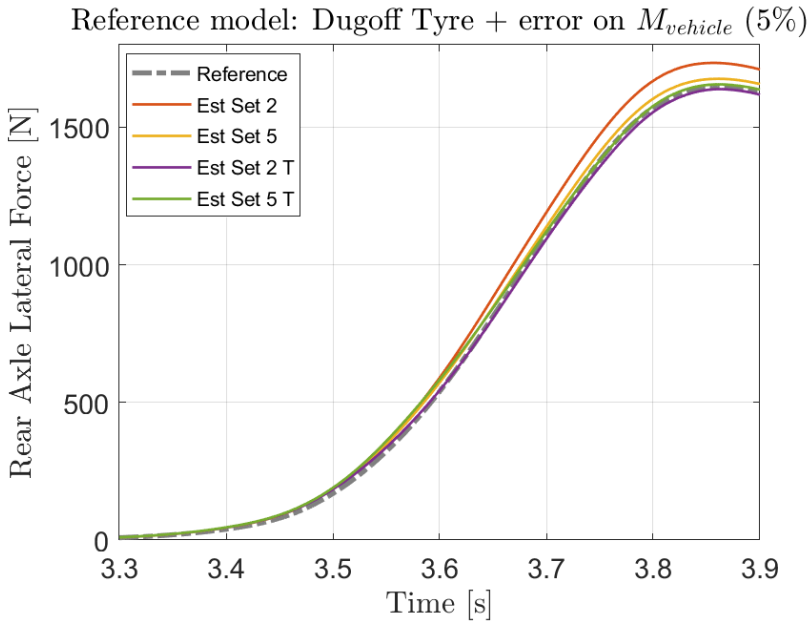

(b) Build-up zoom

Figure 7.27: Rear Axle Load Estimation Tuned. Dugoff tyre reference model + error on car mass

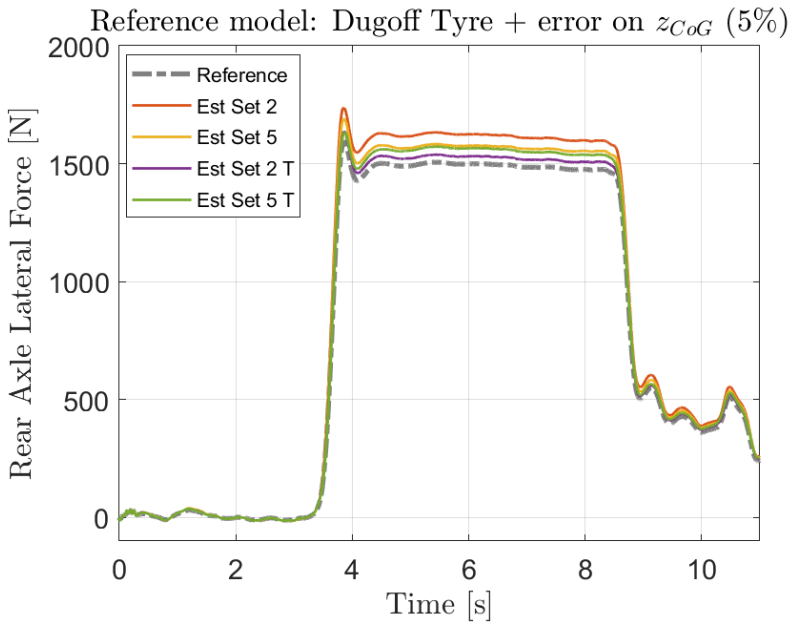

(a)

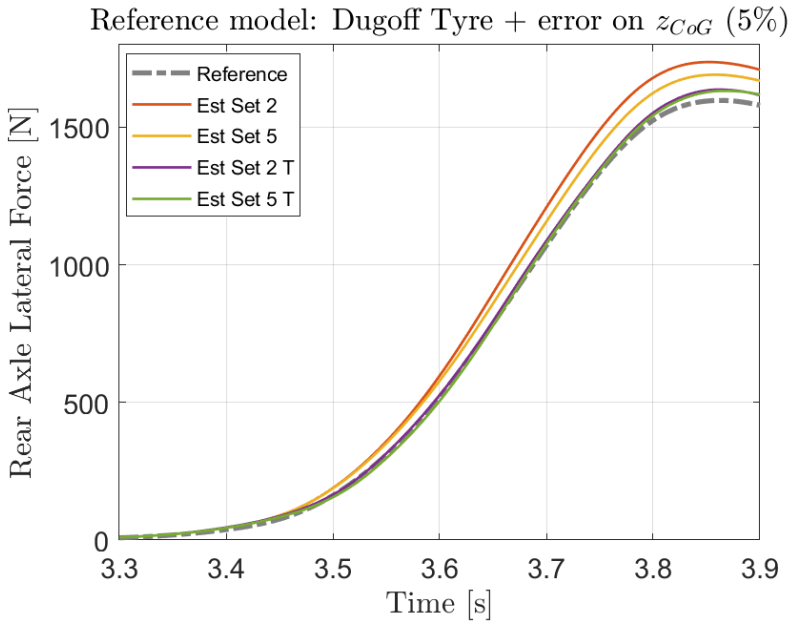

(b) Build-up zoom

Figure 7.28: Rear Axle Load Estimation Tuned. Dugoff tyre reference model + error on CoG heigh

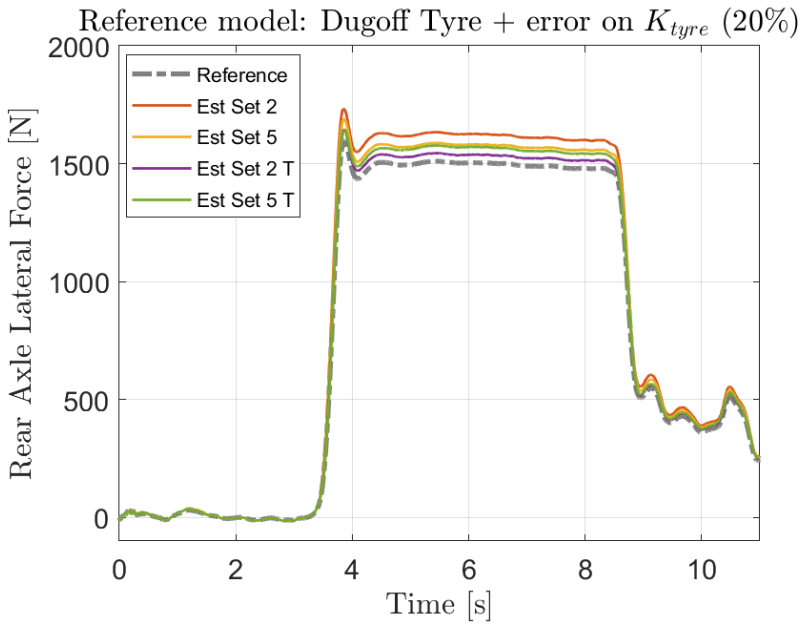

(a)

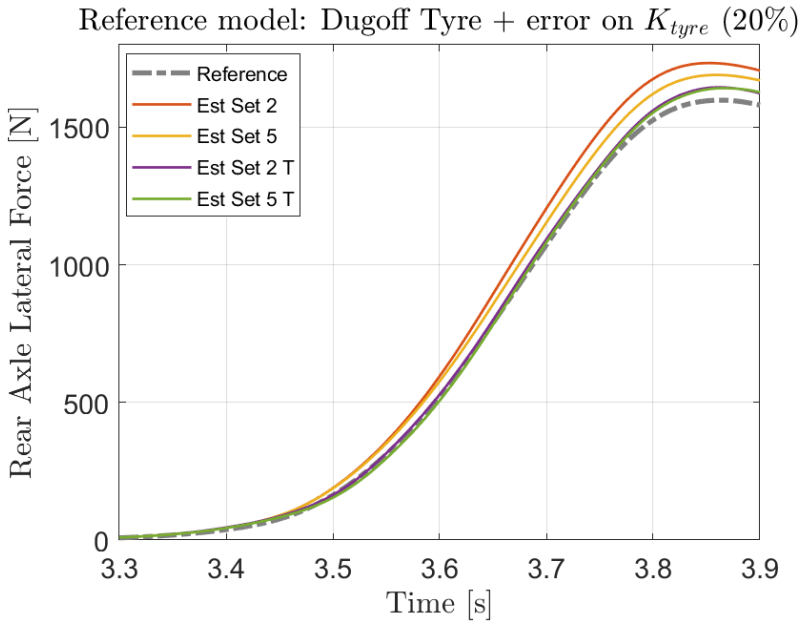

(b) Build-up zoom

Figure 7.29: Rear Axle Load Estimation Tuned. Dugoff tyre reference model + error on tyre stiffness

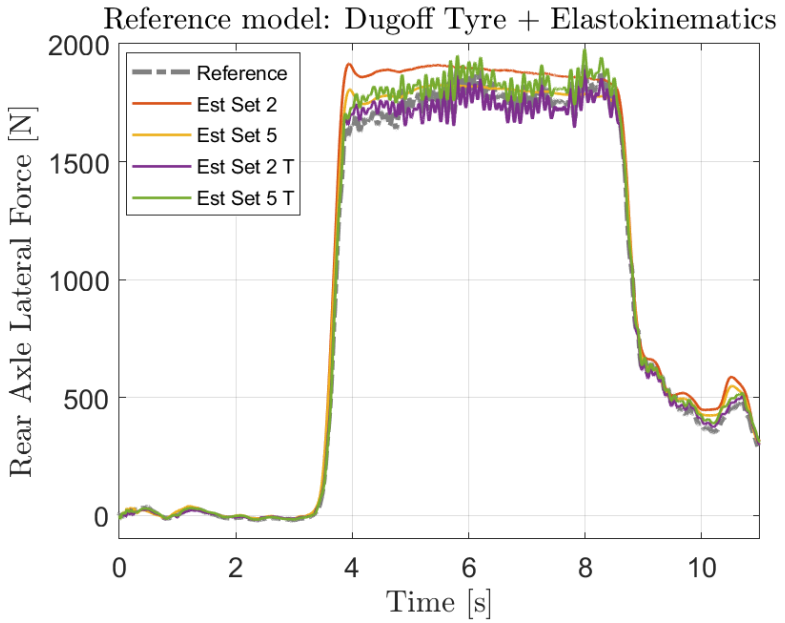

(a)

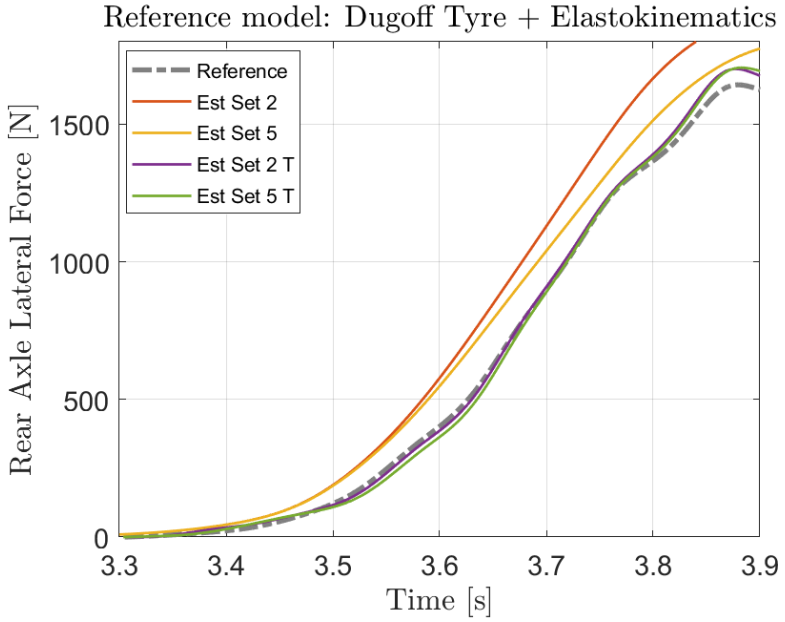

(b) Build-up zoom

Figure 7.30: Rear Axle Load Estimation Tuned. Dugoff tyre reference model + elastokinematics

Chapter 8

Conclusions and Future Works

Model-based virtual sensing presents a promising and innovative approach for the accurate estimation of wheel forces in vehicle dynamics testing. This methodology brings several advantages over traditional Wheel Force Transducers (WFTs) by eliminating the need for invasive modifications to the vehicle, thereby reducing costs and making it more convenient for routine testing and evaluation scenarios. The development and utilization of mathematical models in the model-based virtual sensing process provide insights into tire behavior and contribute to improved vehicle testing and development.

Previous studies have utilized simplified models like the bicycle model to estimate tire forces, but these models have limitations in accurately capturing tire behavior and cornering stiffness variations. More recent research has explored more complex models, such as a 15 Degrees of Freedom vehicle model, to enhance accuracy and enable single wheel load estimation. This work went in the direction, providing some proofs of the effective improvements in using a 15DoFs model, mainly in accuracy of the estimation in transient behaviour.

To ensure accurate and reliable estimation, the use of complex models incorporating the physical properties of the vehicle and tyres is crucial. Additionally, observability analysis plays a pivotal role in identifying the states that can be accurately estimated based on the available measurements, allowing for effective estimation algorithms and appropriate sensor configurations. Careful selection of sensor sets is also vital in model-based virtual sensing. By considering factors such as cost, instrumentation time and availability, a well-designed sensor set can provide optimal performance while minimizing resource requirements.

Future works can involve studying the impact of variations in tire model parameters, suspension characteristics, and sensor calibration on load estimation

performance. This analysis can help to develop guidelines for selecting appropriate parameter values and calibration procedures to improve the robustness and reliability of virtual sensing algorithms. Furthermore, research efforts can be directed towards developing adaptive algorithms that can automatically adjust model parameters based on online measurements and feedback. This adaptive approach can enhance the adaptability and accuracy of load estimation under varying operating conditions and dynamic scenarios. Other insights could come investigating advanced algorithms and sensor configurations that enable the estimation of individual wheel forces (the 15DoFs model has the potential to do it). This can provide valuable insights into the behavior of each tire and its contribution to overall vehicle dynamics. Individual force estimation can help identify tire-specific issues such as imbalanced forces or suspension problems, leading to more targeted diagnostics and improvements in vehicle performance and safety. To support these future research directions, experimental validation studies using controlled test setups and real-world vehicle testing can be conducted.

Overall, model-based virtual sensing represents a significant advancement in the field of vehicle dynamics testing, offering a cost-effective, real-time and accurate solution for estimating wheel forces. With the integration of complex models, observability analysis and thoughtful sensor selection, virtual sensing techniques can greatly enhance the understanding of vehicle behavior, leading to improved performance evaluation and safety assessment.

Bibliography

[1] H. Pacejka. *Tire and Vehicle Dynamics*. Butterworth-Heinemann, 2012 (cit. on p. 1).

[2] Kistler. *Vehicle dynamics, durability and tire testing*. 2018. URL: `https://www.kistler.com/IT/en/vehicle-durability-testing/C00000076` (cit. on p. 1).

[3] M. Viehweger et al. «Vehicle state and tyre force estimation: demonstrations and guidelines». In: *Vehicle System Dynamics* 59.5 (2021), pp. 675–702 (cit. on p. 2).

[4] B. Forrier, W. Desmet, and F. Naets. *Virtual Torque Sensing: A Model-based Approach for Indirect Measurement of Dynamic Operational Loads on Mechatronic Powertrains*. 2018-04-26 (cit. on p. 2).

[5] M. Acosta Reche, S. Kanarachos, and M. Blundell. «Virtual Tyre Force Sensors: An Overview of Tyre Model-based and Tyre Model-less State Estimation Techniques». In: *Proceedings of the Institution of Mechanical Engineers Part D Journal of Automobile Engineering* In press. (Sept. 2017) (cit. on p. 2).

[6] M. Acosta and S. Kanarachos. «Optimized Vehicle Dynamics Virtual Sensing Using Metaheuristic Optimization and Unscented Kalman Filter». In: *Evolutionary and Deterministic Methods for Design Optimization and Control With Applications to Industrial and Societal Problems*. Springer International Publishing, 2019, pp. 275–290 (cit. on p. 2).

[7] L. Ruga, E. Risaliti, S. Ottaiano, and T. Geluk. «A virtual sensing approach for vehicle dynamic performance analysis». In: (2021) (cit. on pp. 3, 26, 27).

[8] D. Simon. «Nonlinear Kalman filtering». In: *Optimal State Estimation*. John Wiley & Sons, Ltd, 2006. Chap. 13, pp. 393–431. ISBN: 9780470045343 (cit. on pp. 6, 17).

[9] T. Blochwitz et al. «Functional Mockup Interface 2.0: The Standard for Tool independent Exchange of Simulation Models». In: Sept. 2012 (cit. on p. 8).

[10] Y. Kawano and T. Ohtsuka. «PBH tests for nonlinear systems». In: *Automatica* 80 (2017), pp. 135–142. ISSN: 0005-1098 (cit. on p. 12).

[11] R. Hermann and A. Krener. «Nonlinear controllability and observability». In: *IEEE Transactions on Automatic Control* 22.5 (1977), pp. 728–740 (cit. on p. 13).

[12] T. Devos, M. Kirchner, J. Croes, W. Desmet, and F. Naets. «Sensor Selection and State Estimation for Unobservable and Non-Linear System Models». In: *Sensors* 21.22 (2021). ISSN: 1424-8220. URL: https://www.mdpi.com/1424-8220/21/22/7492 (cit. on pp. 13, 15).

[13] P. Huang, H. Meyr, M. Dörpinghaus, and G. Fettweis. «Observability Analysis of Flight State Estimation for UAVs and Experimental Validation». In: *2020 IEEE International Conference on Robotics and Automation (ICRA)*. 2020, pp. 4659–4665 (cit. on p. 14).

[14] S. Borguet and O. Leonard. «The Fisher Information Matrix as a Relevant Tool for Sensor Selection in Engine Health Monitoring». In: *Int. J. Rotat. Machine.* 2008 (Jan. 2008) (cit. on pp. 16, 17).

[15] James H. Taylor. «The Cramer-Rao estimation error lower bound computation for deterministic nonlinear systems». In: *1978 IEEE Conference on Decision and Control including the 17th Symposium on Adaptive Processes*. 1978, pp. 1178–1181 (cit. on p. 17).

[16] H. Dugoff, P. S. Fancher, and L. Segel. «An Analysis of Tire Traction Properties and Their Influence on Vehicle Dynamic Performance». In: *International Automobile Safety Conference*. SAE International, Feb. 1970 (cit. on p. 29).